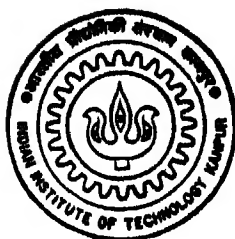


DEVELOPMENT OF CHANNELING FACILITY AND STUDY OF PLASMA INDUCED DAMAGE IN Si AND GaAs

by
ROY PAILY



MATERIALS SCIENCE PROGRAMME

INDIAN INSTITUTE OF TECHNOLOGY KANPUR

FEBRUARY, 1996

DEVELOPMENT OF CHANNELING FACILITY AND STUDY OF
PLASMA INDUCED DAMAGE IN Si AND GaAs

A Thesis Submitted
in Partial Fulfillment of the Requirements
for the Degree of

MASTER OF TECHNOLOGY

by

ROY PAILY

to the
DEPARTMENT OF MATERIALS SCIENCE PROGRAMME
INDIAN INSTITUTE OF TECHNOLOGY KANPUR
February 1996

27 MAR 1996
CENTRAL LIBRARY.
I. I. T., KANPUR

Acc. No. A. 121242

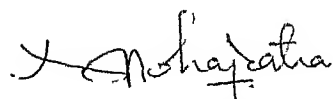
MSP-1996-M-PAI-DEV



A121242

CERTIFICATE

It is certified that the work contained in the thesis entitled
" DEVELOPMENT OF CHANNELING FACILITY AND STUDY OF PLASMA INDUCED
DAMAGE IN Si AND GaAs " by ROY PAULY, has been carried out under
our supervision and that this work has not been submitted
elsewhere for a degree.



Dr. Y. N. MOHAPATRA

Materials Science Programme

I I T - Kanpur

February 1996



Dr. V. N. KULKARNI

Department of Physics

I I T - Kanpur.

February 1996

15/2/96
a=

to JOSEPHINE,

whom I love

ACKNOWLEDGEMENT

The proverb says: " He that waits on his master shall be honoured ". This is true in my life in relation with my supervisors, Dr. V. N. Kulkarni and Dr. Y. N. Mohapatra. I do not have words to describe all I gained from their experience and knowledge. My introduction to the field ion channeling in crystal lattices was entirely due to their encouragement. I am greatly indebted to them for their valuable guidance throughout the programme.

I am also deeply grateful to Sankar and Tapo for their co-operation and help at various stages of my work starting the day one. They patiently gave their time as and when required.

I wish to thank

Giri and Bishaka for their advices and assistances when I most needed.

Gupta and Neeraj who often shared their time and company during my experiments

My thanks also to Mr. Gupta, Mr. Masood, Mr. Rajputh and Mr. Shivprakash who helped to my experiments possible

I must thank the staffs in the Physics Workshop for making the accessories for the goniometer

I owe much to my brothers and sisters who encouraged me by their prayers.

Finally, I praise my Heavenly Father for His goodness and faithfulness all through my journey.

ABSTRACT

The combination of Rutherford back scattering and channeling plays an important role in material analysis for a large variety of studies involving thin films and crystals, specifically in semiconductor technology. The channeling effect in crystals has been turned into a remarkably powerful analytical technique since the channeled component of a beam of energetic ions acts as a probe to detect disorder and displaced atoms, either host or impurity. This work was primarily undertaken to develop and test a modern channeling facility in our institute. Further, in this study we monitored the damage created by the low energy plasma irradiation by channeling set-up in conjunction with the resistivity measurements. Such low energy irradiations of Ar, N, F etc. are integral part of plasma etching processes used in advanced lithographic techniques. However low energy plasma etching introduces damage in the near surface region of the crystal. A precision stepper motor controlled sample manipulator provides the required rotations and translational motions. A suitable vacuum chamber has been fabricated with arrangements for sample mounting, secondary electron suppression and detector holder. The system was demonstrated to be suitable for characterization of high quality crystals. Channeling measurements have been performed using commercially available p-type Si (100) and p-type GaAs (100) single crystals. The parameters χ_{min} , $\psi_{1/2}$ and the thickness of layers (L) contributing to surface peak were measured and these values are in reasonable agreement with the theoretically calculated ones. Low energy nitrogen irradiation was done using a DC plasma immersed ion implantation set-up using arc voltage of 2 KV. The damage induced in

Si and GaAs due to this process has been studied by measuring the different parameters mentioned above. The effect of isochronal annealing has been studied to monitor the recovery of the damage.

The channeled spectra for low energy nitrogen plasma irradiated Si and GaAs samples give disordered layers of thickness 120°A and 66°A respectively. The observed x_{min} values are 23 % for Si and 9.3 % for GaAs. For Si this value is significantly larger than the calculated values (6.7 % for Si), indicating the presence of extended defects below the surface. RBS analysis of the nitrogen peak for Si spectrum gives an irradiation dose of 7×10^{16} atoms / cm². The order of magnitude agrees with the expected dose calculated from the plasma irradiation parameters. The nitrogen peak is located at a depth of 800°A which is about 10 times deeper than the range calculated using TRIM. This is attributed to the channeling of nitrogen ions in Si crystal. The disorder of near surface region decreases with increase in annealing temperature. The channeling parameters (x_{min} etc.) showed systematic improvement in their values after isochronal annealing. However complete damage recovery did not take place after 400°C anneal. The sheet-resistivity which became unmeasurable after nitrogen irradiation was restored to its original value after annealing at 400°C.

CONTENTS

List of figures

List of tables

Chapter 1 INTRODUCTION

Chapter 2 ION BEAM ANALYSIS

- 2 1. Facility for RBS
- 2.2. RBS and RUMP
- 2.3. TRIM
- 2 4 Ion channeling technique
- 2.5. Channeling concepts useful in damage analysis

Chapter 3 EXPERIMENTS

- 3.1. Crystal cleaning
- 3.2. Channeling experiments
- 3.3. Plasma source ion implantation
- 3.4 Furnace annealing of samples
- 3 5. Four-point probe resistivity measurements

Chapter 4 RESULTS AND DISCUSSION

- 4 1. Channeling on as-received samples
- 4.2. Channeling in plasma irradiated samples
- 4.3. Four-point probe resistivity results
- 4.4 Recovery of surface damage

Chapter 5 SUMMARY AND CONCLUSIONS

Appendix Program to calculate channeling parameters

LIST OF FIGURES

- 2.1. Schematic diagram of an RBS system.
- 2.2. Layout of the Van de Graaff accelerator facility at the Central Nuclear Laboratory, IIT Kanpur
- 2.3. Details of RBS chamber.
- 3 1. UHV Sample Manipulator.
- 3.2. Details of the channeling chamber.
- 3.3. DC Plasma Immersed Ion Implantation Set up.
- 3 4. Two-Point Probe Arrangement for resistivity measurement
- 4 1a Schematic drawing of the scattering geometry in channeling experiments.
- 4.1b Scattering yield from the surface of the GaAs (100) crystal as a function of rotation angle R_1 .
- 4.1c. Orientation of major planes around the $\langle 100 \rangle$ in cubic crystals.
- 4.2. Location of the planar minima on polar coordinates for tilts (R_1) 4° and 6° in GaAs (100).
- 4.3a. Aligned and random RBS spectra of as-received Si (100).
- 4 3b. Aligned and random RBS spectra of as-received GaAs (100).
- 4.4 Back scattering spectra and angular yield profile.
- 4.5a. Angular yield profile for as-received Si (100)
- 4.5b. Angular yield profile for as-received Gads (100).
- 4.6. Aligned and Random spectra for 2 KeV nitrogen implanted Si.
- 4 7a. TRIM calculations showing the range of nitrogen ions in Si (100).
- 4.7b. TRIM calculations showing the distribution of vacancies produced in Si for 2 KeV nitrogen ions.
- 4.8. Simulated surface peak for aligned RBS spectrum of 2 KeV nitrogen irradiated Si.
- 4.9. Aligned RBS spectra for the 300°C and 400°C annealed Si(100).
- 4.10a. Simulated surface peak for aligned RBS spectrum of 300°C annealed Si.

- 4.10b Simulated surface peak for aligned RBS spectrum of 400°C annealed Si.
- 4.11. Angular yield profiles for the Si (100) samples :
 - a) As-received, b) 2 KeV nitrogen implanted,
 - c) 300°C annealed d) 400°C annealed.
- 4 12. Aligned and Random RBS spectra for 2 KeV nitrogen implanted GaAs (100).
- 4 13. Simulated surface peak for aligned RBS spectrum of 2 KeV nitrogen irradiated GaAs.
- 4.14. Aligned RBS spectra for the 300°C and 400°C annealed Si(100).
- 4.15a. Simulated surface peak for aligned RBS spectrum of 300°C annealed GaAs.
- 4.15b. Simulated surface peak for aligned RBS spectrum of 400°C annealed GaAs.
- 4.16. Angular yield profiles for the GaAs (100) samples .
 - a) As-received, b) 2 KeV nitrogen implanted,
 - c) 300°C annealed d) 400°C annealed
- 4 17a Fraction of disorder remaining as a function of annealing temperatures in Si (100).
- 4.17b Fraction of disorder remaining as a function of annealing temperatures in GaAs (100).

LIST OF TABLES

- 4.1. Comparison of measured and calculated values of χ_{\min} for as-received Si (100) and GaAs (100).
- 4.2. Comparison of measured and calculated values of $\psi_{1/2}$ in Si (100) and GaAs (100).
- 4.3. The measured and calculated values of the effective number of layers contributing the surface peak in Si (100) and GaAs (100).
- 4 4. The thickness of the disordered layer in Si(100) after 2 KeV nitrogen plasma treatment.
- 4.5. The χ_{\min} and $\psi_{1/2}$ measured in silicon samples.
- 4.6. The thickness of the disordered layer in GaAs (100) after 2 KeV nitrogen plasma treatment.
- 4 7. The χ_{\min} and $\psi_{1/2}$ measured in gallium arsenide samples.
- 4 8. The Four-Point Probe sheet-resistivity values for Si and GaAs samples.

CHAPTER 1

INTRODUCTION

The interaction of energetic ions with solids has been studied for many reasons. Ion implantation has proved to be extremely useful in advance materials processing and integrated circuit fabrication. However the process leads to generation of defects, which unless removed, degrade semiconductor device performance. The nature and types of defects created vary widely depending on the mechanisms of interaction. Ion-solid interactions are generally divided into nuclear and electronic contributions. The former denotes the energy loss by collisions between the ions and the core of the target atoms while the later involves losses due to electron-hole creation or excitations generated when ions travel in the electron media. This understanding of high energy collisions (> 100 keV) involving light ions is mature because nuclear and electronic contributions to the stopping power can be decoupled in theoretical formulations and the traces of high energy ions can be measured [1]. However an accurate descriptions at low and medium energy (< 10 keV) is not well studied. In this case, the nuclear and electronic stopping powers depend on atomic and electronic structures of the the target and their effects are closely correlated. Moreover the size of defects generated by low energy ions is in the order of nanometers, and require high precision probes to resolve such features [2]. Channeling effect is a remarkably powerful analytical technique. It provides simple and direct values for the amount of lattice disorder and location of the implanted atoms.

Channeling phenomenon was first discussed and predicted in 1912 by Stark. His paper on the subject was ignored and forgotten, however, perhaps due to a lack of instrumentation. With the birth of atomic and nuclear physics, half a century later, this phenomenon was rediscovered by Robinson and Oen [3] during a computer simulation on the directional dependence of the penetration depth of charged particle in single crystal solids. Experimental evidence for channeling was obtained almost simultaneously in different laboratories during 1963. In 1965 Lindhard gave a theoretical description of channeling phenomenon. He argued that charged particles penetrating a single crystal along or near a major axis experience a collective string potential produced by the rows of atoms along that axis. If the incident direction of the ion beam is nearly parallel with the string of atoms, the string potential will steer the charge particle beam forward. A critical angle is defined as the limiting angle between the incident direction and row of atoms such that the steering effect exists. When charged particles are incident in a direction exceeding the critical angle, those particles have transverse kinetic energy exceeding the collective string potential. The collective steering effect subsequently disappears. An excellent review on the theory of channeling effects was given by Gemmell [4]. A detailed description of theory, observation and applications of channeling was collected into a book by Morgan in 1973. Many chapters are devoted to channeling applications. They are applications to radiation damage, surface studies, and to semiconductor technology. Excellent discussions on lattice location of foreign atoms are also included [5].

The present day applications of channeling include the investigations of stacking faults and dislocations in super-lattice structures. The channeling technique can detect a wide range of intrinsic defects including interstitial, dislocations, stacking faults, micro twins, and amorphous clusters. Resonance channeling and catastrophic dechanneling and channeling radiation are some of the effects of channeling utilized in applications. In Fermi laboratories channeling through strained layer crystals is utilized to deviate the GeV beams which on the other hand is not possible because of the huge magnetic field requirements.

Application of channeling has assumed significance in the study of interfaces and modulated layer structures. Interface relaxation, strain and contraction of various superlattices have been studied. Channeling is a sensitive tool in the study of lattice location of impurity atoms at substitutional or interstitial sites. Clustering of substitutional impurity atoms show displacement of the impurity atoms from lattice sites due to the change of bond distance. Channeling can be used to measure impurity displacement as small as 0.1 \AA [6].

At high defect densities the ion channeling / back scattering technique can give the depth distribution of defects with a resolution of approximately 10 nm. Quantitative analysis of the defect depth profile requires that a single type of defect dominates the scattering of particles out of channeling trajectories. This scattering process is characterized by two defect-specific quantities

the direct scattering factor and the dechanneling cross-section. It is possible to distinguish one type of defect from another by carefully studying the energy dependence of dechanneling. The dechanneling interpretation is not always unique, and in practice it is difficult to obtain structure information through that method. Despite these negative qualities, channeling has emerged as an attractive and unique method in certain defect studies. Defects created in semiconductor materials during various process steps [7,8,10] is one such area which is of considerable current interest.

Objectives of this work :

In view of the technological importance of channeling experiments as a probe in crystal lattice studies as described above, the first and main objective of this work has been to develop a channeling set-up along with the Rutherford back scattering system in our laboratory. The second objective has been to study the damage introduced by low energy nitrogen ions in Si and GaAs single crystals using channeling in conjunction with electrical measurements. The importance of such a study lies in the process of plasma etching, which is used as dry development process in advance lithography technique. This etching tool is of great significance because the device dimensions can be reduced.

Conventionally, Si and its compounds can be patterned using wet chemicals such as hot phosphoric acid. However, wet etching methods result in isotropic etching profile, which make very difficult

to achieve feature sizes less than 3 μm . Therefore plasma etching is used almost exclusively in the modern microelectronic fabrication technology owing to its etching anisotropy. This anisotropy results from the ion bombardment of the substrate surface during etching, which enhances the etching in the vertical direction [9]. However the plasma etching results in damage in the near surface region of the crystal and this damage unless removed by a suitable method, degrades the device performance. Generally the structural damage and the electrical properties are recovered by suitable annealing steps. In the area of low energy ion bombardment, structural damage and its recovery, and the recovery of electrical properties are the two aspects which have not received adequate attention. Therefore as mentioned above, the second objective of this work has been chosen to study the damage in Si and GaAs crystals subjected to low energy nitrogen irradiation in a DC arc plasma system.

The next chapter gives some important aspects of ion beam analysis. The details of the experiments, especially the channeling set-up and the goniometer (sample manipulator) characteristics are presented in chapter 3. The results of performance test of the goniometer using as-received Si and GaAs samples followed by the channeling studies on these samples subjected to the low energy nitrogen irradiation in a DC arc plasma are discussed in chapter 4. The effects of annealing on the damage recovery and the electrical properties are also presented. The conclusion of the work are presented in chapter 5.

CHAPTER 2

ION BEAM ANALYSIS

Ion beams used for both material modification and analysis. There are several excellent texts and reviews on the subject [1,14,30]. The text by Feldman gives a comprehensive introduction to some common analysis techniques using ion beams [14]. The Rutherford Back scattering technique is one of the most frequently used techniques for quantitative analysis of composition, thickness and depth profiles of thin solid films or solid samples near the surface region. Due to its simplicity, versatility and amount of information it can derive in a short data acquisition time it has evolved in the past few years into a major materials characterization tool [13].

2.1. FACILITY FOR RBS

The basic requirements for RBS measurement is given in Fig. 2 1. The requirements for RBS are :

1. A particle accelerator to provide required energetic charged particles eg. 2 MeV Van de Graaff accelerator,
2. An ion source which provides ions of desired gaseous species,
3. A scattering chamber described below,
4. A computer simulation package to analyze the data.

The 2 MeV Van-de-Graaff accelerator facility has been utilized in this work. The lay-out of the Van-de-Graaff facility at

the Central Nuclear Laboratories in IIT Kanpur is shown in Figure 2.2. The accelerator has been described in detail by Banerjee [11] and Chaudhuri [12]. This accelerator is a belt type electrostatic generator. Inside the accelerator there is a closed conducting shell, which serves as the high voltage terminal. If one deposits charge on the inside surface of the shell, the charge accumulates on the outside surface. An insulating belt moves through this shell. Electrons are constantly removed from the belt on the side away from the high voltage terminal, by applying a positive potential. To prevent the sparking the whole assembly is enclosed in a pressure vessel containing an insulating mixture of nitrogen and carbon-dioxide at about 340 psi pressure.

Fig 2.3 gives the details of the RBS chamber. This chamber is mounted on a diffusion pump vacuum system with a liquid nitrogen trap which yields a vacuum of the order of 10^{-6} torr. The samples are mounted on a sample holder. A suppressor which is connected to a -ve potential is used to suppress the secondary electron emission. In the absence of the suppressor the secondary electron emission can interfere the measurement of the total charge. The textbooks by Chu et al [13] and Feldman et al [14] give a comprehensive account of RBS.

The Helium ion beam is collimated before entering the RBS chamber by a X-Y slit arrangement to obtain a beam spot of about 1mm x 1mm dimensions. The detector is mounted at a scattering angle of 150° and subtends a solid angle of 2.57 milliradian at the center of the beam spot. The silicon surface barrier detector is mounted on a

cylinder cooled by circulating chilled water. This helps in the reduction of the leakage current in the surface barrier detector from 200nA to 50nA. The detector is kept at a bias of +100V. The electrical signals from the surface barrier detector are analyzed by the usual nuclear electronics and multi channel analyzer. The height of the signal gives the energy of the detected particle. A plot of the energy of the particles versus the frequency of occurrence of the signal is called as a "spectrum" which contains the information regarding the elements and their depth distribution in the sample. In these measurements an EG&G ORTEC 142A preamplifier, 572 Amplifier and gated biased amplifier an ND65 PC multi channel analyzer connected to a PC were used

2.2 RBS and the RUMP Simulation Package

In this work the software package RUMP has been used for analysis. The RUMP (Rutherford Universal Manipulation Program) simulation program has been developed at the Cornell university by Doolittle and co-workers [15]. In the simulation, a theoretical sample structure consisting of several layers of varying thickness is first prepared. The experimental parameters are fed in to the program. A back scattering spectrum thus constructed is compared with the experimental spectrum. This procedure is used iteratively to arrive at the best set of parameters so that the simulated spectrum compares well with the experimental data.

The theoretical calculations of nitrogen ion ranges and damage was performed using TRIM (Transport and Range of Ions in Matter) computer package developed by Ziegler et al.[16,17]. The nuclear energy deposited by the projectile ions to the target {Si(100) & GaAs(100) crystals} was calculated using this program. The program input consists of ion mass and energy, the details of the layer structure, the displacement energy of the lattice atoms (E_d) and the binding energy (E_b). The details are given in the the book by Ziegler [11]. If Z_1 and E_1 are the atomic number and the energy of the incident ion, Z_2 is the atomic number and E_2 the energy acquired by the target atom after a collision event with the incident ion, the following can be the consequences under different conditions:

Condition	Consequence
$E_1 > E_d, E_2 > E_d$	A vacancy results
$E_1 < E_d, E_2 < E_d$	E_2 is released in the form of phonons
$E_1 < E_d, E_2 > E_d$	Original atom remains at the site The event is called a Replacement Collision
$Z_1 \neq Z_2$	Z_1 becomes an anti site atom
$Z_1 = Z_2$	Z_2 merely replaces Z_1 in the cascade and E_1 is released as phonons
$E_1 < E_d, E_2 < E_d$	Z_1 becomes an interstitial and $E_1 + E_2$ is released as phonons

The TRIM program has the provision of performing calculations for a maximum of 3 layered structure only. The range of the nitrogen ions is shown in Figure 4.7a & 4.7b. This gave the range and final distribution of the nitrogen ions. During irradiation the energy of the ion beam fluctuated by around 10%. So the values calculated thereof are accurate to only within 10%.

2.4 ION CHANNELING TECHNIQUE

This provides an introduction to the use of channeling for defect studies. Here we briefly describe ion channeling and the associated concepts which make it useful for defect analysis and surface studies.

2.4a Origins of the Channeling effect :

When ions impinge on a disordered solid or a misaligned single crystal they encounter the atoms at random and sample a random distribution of impact parameters [13,14]. However, if the bombarded sample is a single crystal aligned so that the ions are incident parallel to an axial or planar "channel", then ions experience successive, correlated collisions with the systematically arranged atoms and acquire oscillatory trajectories in the open regions, or channels, between the rows or planes of atoms. The minimum distance of approach of a channeled ion to atoms on normal lattice sites is ρ_{min} approximately 10^{-9} cm. Since many ion-solid interactions such as Rutherford scattering require much closer impacts ρ approx. 10^{-12} cm, the reduction in the yield of these phenomena become sensitive monitors of crystal perfection.

Several consequences of channeling can be exploited for defect studies in single crystals. When a beam of ions is incident parallel to an axial direction in a single crystal approximately 97 % of the ions impact at a distance $> \rho_{min}$ from the atoms which terminate the rows of atoms at the surface. These ions acquire oscillatory trajectories within the channels whose amplitudes of oscillation are determined by their initial impact parameters [5]. The fraction of ions which impact within ρ_{min} will either interact directly with the surface atoms (surface scattering) or be deflected through too large an angle to be confined to a channel and assume random trajectories with normal interaction probabilities. This interaction fraction of the beam which impacts within ρ_{min} is the least yield reduction you can hope to achieve for a perfect crystal and is called the minimum yield. In its simplest form it can be expressed.

$$\chi_{min} = N d \pi \rho_{min}^2$$

where N is the number of atoms /cm³ of the target

d is the spacing in cm between atoms along the axial row of atoms

Those particles which are initially channeled become sensitive to disorder in the bulk of the crystal either by direct back scattering from displaced atoms, or they can be dechanneled by thermally vibrating or displaced atoms

2 4b EXPERIMENTAL ARRANGEMENTS .

Numerous experimental geometries have been utilized in channeling studies and various phenomena (ion scattering, nuclear reactions, x-rays, energy loss, etc.) have been exploited as sensors [6] Four frequent arrangements are given below

2.4b(1) Single Alignment(Channeling) :

This is the most common experimental set up utilized in damage analysis. The acceptance angle of the detector ψ_d is much greater than the critical angle for channeling ψ_c . Our experiments are done in this arrangement. The major advantages of single alignment geometry are that it is simple, compact, easily interpreted and requires very small beam currents {approximately $0.1 - 10 \times 10^{-9}$ amps.}

2 4b(2) Forward Scattering :

When we go to the forward scattering angles, the beam current needed for analysis is reduced because of the angular dependence of the Rutherford scattering effect [18] With proper detection geometry, knock-on forward recoil scattering can be exploited to depth profile light impurities in heavy hosts.

2 4b(3) Transmission :

Channeling studies of ions transmitted through thin single crystals have provided insights and understandings of the phenomenon which are essential for its use as a damage analysis tool [19]. It has been possible to study the dependence of stopping powers, impact

parameters, potentials for channeled ions as well for dechanneled ions. It has also yielded detailed understanding of the flux distributions, multiple scattering phenomena etc.

2 4b(4) Double Alignment (Channeling and Blocking) :

In double alignment geometry an analysis detector with an acceptance angle ψ_c much smaller than the critical angle ψ_b for blocking is aligned with a major axis or a plane. Consequently when the ion beam is incident along a channeling direction only the minimum yield fraction approximately χ_{min} interacts with atoms on normal lattice sites because of the channeling effect, and only approximately χ_{min} of this fraction { i e χ_{min}^2 } reaches the double alignment detector because of the blocking effect. Thus the background level for scattering from a perfect lattice is reduced from χ_{min} approximately $2 \cdot 10^{-2}$ to 10^{-3} by going from the single to double alignment geometry, and this improves the the sensitivity for detection of displaced atoms in defect studies and in lattice location investigations.

2.5 CHANNELING CONCEPTS USEFUL IN DAMAGE ANALYSIS

2.5a Surface Scattering :

Ion channeling provides a special sensitivity to both quantity and geometrical positions of atoms located at the surface of single crystals. When a beam of ions is incident parallel to an axial direction, the atoms on the surface have a normal scattering probability. The sub surface atoms on the other hand are shadowed by the surface atoms and have a greatly reduced scattering probability. So in the spectrum we see a surface peak. The area under the surface peak is a direct measure of the number of atoms exposed to the incident beam. Similarly, the surface disorder increases the surface peak yield. The yield of scattered ions results from direct back scattering events before any channeling can occur and is thus easily interpreted.

It is possible to utilize ion beams of various energies for structural determination of surfaces. Just as the angular variation of the yield of ions scattered from defects in the bulk can be used to determine their lattice sites, so the angular variation of the surface peak yield can be utilized to determine the geometrical arrangement of surface atoms relative to the bulk. The magnitude of the increase in yield, and the magnitude and sign of the angular minimum provide an accurate characterization of relaxed surfaces.

2.5b Yield Oscillations

The variations in the scattering yield directly behind the surface peak are referred to as yield oscillations [20]. They occur for ions directed along both axial and planar channels and originate from the variation in ion flux with depth (and angle) induced by the channeling effect. The ions which impact beyond ρ_{\min} of the atoms acquire oscillatory trajectories within the channel. These discrete oscillatory trajectories have wavelengths and amplitudes within the channel determined by their transverse energies, and it is the distribution of these trajectories which determines the ion flux within the channel.

The yield oscillations are most clearly illustrated in planar channeling. Those ions with large amplitudes of oscillation within the planar channel approach closely to the planes of atoms every $\lambda/2$ where λ is the wavelength of oscillation in the channel, and these ions have an increased probability for scattering at that depth. So the ions scatter selectively at certain depths. Since the scattering energy can be converted to depth if the channeled stopping powers are known, the peak positions represent direct measurements of the wavelengths of the channeled trajectories. The converse is also true. The stopping powers utilized in depth conversions, determined from correlated transmission measurements.

Similarly axial yield oscillations provide enhanced sensitivities to specific (and predictable) lattice sites, and as such they can be used as selective probes of defect configurations and impurity positions.

2.5c Direct Back scattering and Dechanneling :

Channeling spectra are most easily interpreted when the direct back scattered ions can be easily distinguished from those which become dechanneled and then back scatter. The scattering yield increase behind surface peak is due to the dechanneling of the incident beam. The origin of this dechanneling is the increased angular divergence of the ion beam, due to multiple scattering in the disordered over-layer before entering the crystalline region.

2.5d Background Suppression .

By reducing the background scattering from the host (by placing the detector in a grazing geometry to improve the depth resolution in high resolution case) one can study the surface disorder or light impurities. The oxygen, carbon, nitrogen peaks are visible in the high resolution cases.

2.5e Lattice Location .

The position of the defect or impurity atom is deduced by interpreting the channeled component of the ion beam with the displaced atom [13,14]. The probability that the channeled beam will interact with the displaced depends on :

(a) the magnitude of the displacement { i.e. it must be $> \rho_{min}$ } and the crystallographic orientation of the displacement relative to the incident beam,

- (b) the flux distribution of the channeled beam at the position of the displaced atom, and
- (c) the interaction cross section

2 5f Flux Peaking and Statistical Equilibrium :

Since the channeled particles are excluded from the area $\pi\rho_{\text{min}}^2$ around a string, the flux of particles per unit area in the channel, and thus the probability of interacting with an interstitial atom, is higher than for a randomly directed beam. This is the basis of flux peaking effect and has proved to be so useful in atom location studies. After penetrating a sufficient depth into the crystal, the probability of finding a given ion at a given position is independent of position within the area accessible to it and zero outside that area; this condition is referred to as statistical equilibrium.

2 5g Triangulation :

The flux distribution in the channel also varies with ion energy and angle of incidence of the ions relative to the channeling direction. These variations provide additional sensitivity to the type and location of lattice impurities. In triangulation a comparison of the interaction yields for the host lattice relative to impurity measured along different intersecting crystallographic directions are utilized to pin point defect sites with great accuracy.

3.1 Crystal Cleaning .

The crystals used in this work are device grade Zn-doped GaAs (100) and B-doped Si (100). As a first step we thoroughly de-greased the crystals using trichloroethylene (t.c.e) followed by ultrasonic rinsing in acetone. This cleaning procedure guarantees that any grease on crystals, that might be insoluble in subsequent cleaning steps, are removed.

After surface cleaning, etching of the residual impurities and oxide layer was done. For Si (100) we briefly dipped in the etching solution of composition 2 ml. HF + 15 ml. HNO₃ + 5 ml. CH₃COOH for about 15 seconds. The samples have to be handled using teflon tweezers during this process. This is called planar etch with etch rate 5 $\mu\text{m.}/\text{min}$ [21]. Immediately after etching the wafers were quickly immersed in de-ionized water to remove the residues of etching solution and thus to prevent further etching.

For GaAs (100) the etching solution of composition of H₂SO₄ : H₂O₂ : H₂O in the ratio of 5:1:1 was used. The etching rate is exponential in this case. After etching we used de-ionized water and acetone one after another ultrasonically to remove the residues of etching.

3.2 Channeling Experiments

3.2a Sample Manipulator :

For channeling studies, in order to align the crystal with

respect to the incident He^+ beam, we used Sample Manipulator supplied by High Voltage Engineering Europa which is specially designed for ultra high vacuum systems. The Sample Manipulator is shown in Fig 3.1.

This can rotate a sample around three independent axes by means of two linear movements and one rotary movement, driven by stepper motors. The three axes of rotation intersect at one point on the surface of the sample. The range and resolution of the various rotations are given below:

(1) Rotation 1 (R1)	360°	in steps of 0.018°
(2) Rotation 2 (R2)	200°	in steps of 0.0125°
(3) Tilt (R3)	$\pm 3.5^\circ$	in steps of 0.0071°

In addition to the rotations there are provisions for shifting the sample along three axes

X- $\pm 10\text{mm}$;set point resolution 0.01mm

Y- $\pm 10\text{mm}$;set point resolution 0.01mm

Z- $\pm 10\text{mm}$;set point resolution 0.01mm

This allows the measurements to be done at different locations on the sample during the same run. It is also useful in removing the sample from the beam line, when desired. Initially, the sample manipulator was installed in the horizontal direction. The scattering chamber and accessories were made by Balaji [32]. But the above mentioned specifications are for mounting the manipulator in an upright position only. So we installed it in the vertical position as shown in Fig 3.2.

3.2b Alignment

During the course of this work, the sample manipulator was installed for the first time. This involved stable mounting of the manipulator which weighs about 100 kg. Vacuum compatibility of both the sample manipulator and the specially designed chamber were thoroughly tested.

The first step was to align the beam so that it falls at the center of the sample holder inside the Sample Manipulator. For this we place a small quartz piece of ~ 2 mm dia on the sample holder, so that when beam falls on the quartz it glows. This is necessary to ensure that beam remains at the same position on the sample during various rotations.

A RBS spectrum was then taken with the help of the Multi Channel Analyzer. Keeping R_1 and R_3 constant (for eg: $R_1=333$ i.e 6 degrees & $R_3=0$), yields were taken in an energy window for say 100 counts by varying R_2 values. Both crystals were of (100) type so planar minimum values in the yields observed at 45 degree apart. We repeated the same for a different R_2 value (for eg : $R_1=444$ i.e 8 degrees & $R_3=0$), in this set also planar minimum yields were at 45 degree apart. With the help of a polar graph sheet the planar minima for the two different R_1 values were plotted and the intersection of the corresponding planar lines was taken. By changing R_1 , R_2 & R_3 values, to this coordinates obtained in the point of intersection, the sample is aligned in the axial direction with respect to the incident beam. At this position a spectrum is taken which is called as aligned spectrum.

Next, the scattering yield in a selected energy window was measured as a function of tilt angle (θ) (angular scan) around the major aligned crystallographic axial direction

Orienting the crystal to obtain axial channeling is not as difficult as to orient it so that channeling effects are completely excluded. Therefore, back scattering spectra that coincide with those from an amorphous sample are hard to obtain. For random spectra, we tilted the crystal by an angle $> 6^\circ$ so that the incident beam is well away from the crystallographic axis

3.3 Plasma Source Ion Implantation

The technological importance of ion implantation is well established due to its diverse applications in improving the mechanical, electrical and optical properties of materials. In the ion implantation process the ions are accelerated to high energy (10 keV -- few hundreds of keV) and are injected in a solid. This process not being controlled by thermodynamic constraints, can also be used to produce new localized phases depending on the application.

Plasma Source Ion Implantation (PSII) is relatively a new technique [27] and represents a radical departure from the conventional ion implantation technology. The PSII technique circumvents the inherent line-of-sight restriction as in case of conventional ion implantation. In PSII, targets to be implanted are kept directly in a plasma source and then biased to a high negative potential. A plasma sheath is formed around the target and the ions bombard the entire target. PSII has been used for a variety of semiconductor and metallurgical [24-25] applications

In this work we used the DC plasma source ion implantation facility which has been set up recently for implanting H, D, N ions [22] of 1-6 keV energy. The sketch of plasma source ion implantation chamber is shown in Figure 3.3. The chamber is first evacuated to a base pressure of 10^{-7} torr. using a turbo molecular pump. A flow of nitrogen gas is established in the chamber to provide a final equilibrium gas pressure of 10^{-2} - 10^{-3} torr. The plasma is generated by ionizing the gas with the help of a d.c. glow discharge method and the sample is biased to a negative potential of 2 KV. As the sheath, containing an electric field is formed, it shields the surrounding plasma from the applied potential. Ions within and at the edge of the sheath are accelerated by the electric field and travel through the sheath and are implanted into the sample. Implantations on both Si and GaAs are carried out for a time duration of 6 minutes.

3.4 Annealing of Samples :

Nitrogen plasma damages the surface layers of the crystals. This was confirmed from the four-point probe sheet-resistivity measurement and from the channeling experiments on the implanted samples. Our next step in the experiments was to study how the damaged layers recover during subsequent annealing.

Annealing of the samples were carried out in a clean and high vacuum { 10^{-5} torr.} obtained in a quartz tube holding the samples. Temperature control was achieved by using an Isotherm Temperature Controller which has the ability to control temperature within ± 2 deg centigrade. The temperature measurement was done using a calibrated Chromel-Alumel thermocouple.

The plasma implanted samples were annealed at 300°C and 400°C for 15 minutes each. Then the four-point probe sheet-resistivity (Ω / \square) and channeling measurements were repeated for each annealing step.

3.5 Four- Point Probe Resistivity Measurements :

3.5a Basic Concepts

We used the conventional four probe to measure resistivity (ρ) which is a basic semiconductor material parameter and is defined by $\rho = 1 / \{ q (n v_n + p v_p) \}$ where n and p are free electron and hole concentrations, and v_n, v_p are their mobilities respectively [29]. The resistivity can be measured in a number of ways. The methods range from contactless, through temporary contact to permanent contact techniques. The four-point probe is one of the most common methods for measuring the semiconductor resistivity because two-point probe method are more difficult to interpret. Consider the following two-point probe arrangement in Figure 3 4. Each probe serve as a current and as a voltage probe. The total resistance between the two probes is given by

$$R(t) = V/I = 2 R(c) + 2 R(sp) + R(s)$$

where R_c is the contact resistance at each metal probe/semiconductor contact, $R(sp)$ is the spreading resistance under each probe R_s is the semiconductor resistance. Neither $R(c)$ nor $R(sp)$ can be accurately calculated so that R_s cannot be accurately extracted from the measured resistance.

A solution to this dilemma is the use of four probes. Two probes carry the current and the other two probes are used for voltage sensing. The probes are generally arranged in line with equal probe spacing. Although the two current carrying probes still have contact and spreading resistance associated with them, that is not true for the two voltage probes because the voltage is measured with a high impedance voltmeter which draws very little current. The two parasitic resistances R_c and R_{sp} are negligible because the voltage drop across them are negligibly small due to the very small current that flows through them.

It can be shown that the resistivity is given by

$$\begin{aligned}\rho &= (\pi t / \ln 2) V / I \\ &= 4.532 t (V / I)\end{aligned}$$

where t is the wafer or layer thickness. This equation is valid for $t \ll s / 2$ where s is the probe spacing. For this study since we used the same samples for different treatment (t remains the same), we measured the sheet-resistivity (Ω / \square) for comparison.

3.5b Measurement errors and precautions

(1) Sample Size :

If the wafer or the layer to be measured is appreciably thinner than the probe spacing, which is usually the case, the calculated resistivity varies directly with thickness. It is therefore very important to determine the thickness accurately.

(2) Minority Carrier Injection :

Although the probes constitute metal semiconductor contact,

there is still some minority carrier injection at the current probes. This is generally a small effect but under high current conditions it may not be negligible. To reduce this effect, the surface should have a high recombination rate for minority carriers. This is best achieved by using lapped surfaces. For highly polished wafer it may not be possible to achieve the necessary high surface recombination.

If the voltage probes are sufficiently far from the injecting current probe, even if the minority carriers are injected, they will have decayed by recombination and cause very little error. Minority carrier injection may be important for high resistivity materials. For silicon this applies for $\rho > 100 \Omega \text{ cm}$.

(3) Probe Spacing :

A mechanical four-point probe exhibits small random probe space variations. For small probe spacing variations the correction factor $F_s = 1 + 1.082 (1 - S_2 / S_m)$ where S_2 is the probe spacing, S_m is the mean value of probe spacings. Errors due to probe wander can be reduced by averaging several independent readings.

(4) Current Effects :

The current can affect the measured resistivity in two ways: by an apparent resistivity increase produced by wafer heating and by an apparent resistivity due to minority carrier injection. Surface leakage is reduced or eliminated by enclosing the probe in a shielded enclosure held at potential equal to the inner probe potential.

(5) Temperature Effects .

It is important that the temperature along the sample be uniform in order not to introduce thermoelectric voltages. Temperature gradients can be caused by ambient effects but are more likely due to sample heating by probe current. Current heating is most likely to occur in low resistivity samples where large currents are required to obtain readily measurable voltages.

Temperature corrections are made according to $\rho(t) = \rho(o) / \{ 1 + C(T - T_{ref}) \}$ where $\rho(o)$ is the uncorrected resistivity, C is the temperature coefficient of resistivity, T is the measurement temperature, T_{ref} is the temperature of the reference standard.

(6) High Resistivity Materials .

Materials of high resistivity, such as surface damaged samples in this work or semi-insulating GaAs with $\rho \sim \Omega \text{ cm}$ etc. are difficult to measure by conventional four-point probe method. Moderately doped wafers can become highly resistive at low temperatures and are similarly difficult to measure. Special measurement precautions must be observed.

The simplest measurement method relies on providing the wafer with a large contact on one side and small contacts on the other side of the wafer. A current is passed through the contacts and the voltage is measured. Two terminal measurements are notorious for being complicated by contact effects. One approach to this problem is the guarded approach using high input impedance unity gain amplifiers between each probe on the sample, and the external circuitry. The

amplifiers effectively eliminate the stray capacitance in the leads. This reduces the leakage currents and the system time constant

The weakness of the four-point probe technique is the damage it introduces when the probe comes into contact the surface. The damage is not very large but sufficient not to make measurements on wafers to be used for device fabrication. The probe also samples a relatively large volume of the wafer, preventing high-resolution measurements

3.5c Experimental Arrangement

The experimental set up we have for this measurement consists of:

(a) 6181C DC Hewlett-Packard current source which is capable of supplying 0-250 mA current in voltage range of 0-100 Volts. From this supply we can draw current in steps of 25 μ A.

(b) Model A-4 1.5 mm sample holder (Osaw India) arrangement in which we can arrange the four probes either in a line or in square shape.

(c) Wavetek 1271 selfcal digital multi meter with the following facilities :

selectable 5 & 1/2 to full 8 & 1/2 digits resolution, DC Voltage ranges from 10 nV to 1100 V, true RMS AC Voltages from 100nV to 1100 V, 10Hz to 1 MHz which can be optimized either for high speed or accuracy, 2-wire and 4-wire Resistances from 1 $\mu\Omega$ to 2 G Ω and DC and AC current option

We measured the as-received samples sheet-resistivity (in Ω / \square) first, by taking different sets of currents and voltages

at different portion of sample surfaces and then averaging it. Then, after implantation of both Si and GaAs we noticed an increase of sheet-resistivity of many orders in both samples

Chapter 4

RESULTS AND DISCUSSION

One of the main motivations of this work has been to develop channeling set-up and demonstrate its effectiveness for semiconductor characterization. In the first part of this chapter we present results on as-received silicon and gallium arsenide crystals. We then go on to monitor the damage induced by low energy nitrogen plasma in these crystals and study its thermal recovery using the channeling set-up in conjunction with resistivity measurements. These results are presented in the later part of the chapter.

4.1. Channeling studies on as-received samples

The first step is to align the crystal with respect to the beam direction. Generally all crystals are cut 3° or 4° off from their specified directions, so this crystal alignment is important to make sure that the probing beam is properly aligned with respect to the crystal.

4.1.a. Crystal alignment

A schematic drawing of the geometry is shown in Fig.4.1a. The scattering yield from the surface of the crystal, as a function of rotation angle R_1 is recorded for an integrated charge of $0.1 \mu C$. A part of such a scan obtained for a tilt angle of 6° for as received GaAs sample is shown in Fig. 4.1b. As the crystal rotates, various planes get aligned with the incident beam giving rise to what is known as planar minima in the scattering yield Chu et al page No.227 [9].

Generally the low index planes give rise to pronounced minima in such a scan. For $\langle 100 \rangle$ crystals with a cubic structure, the orientation of the low index planes are shown in 4.1c.

On the basis of this geometry the planes for the minima are identified and are shown Fig. 4.1b. Notice that the angular positions of the minima are 45° apart as expected. And we can see that the $\{110\}$ plane gives a strong dip compared to the $\{100\}$ plane, this is because there are less atoms in $\{110\}$ plane than $\{100\}$ for zincblende structure. Similar scans are taken for different tilt angles and a polar plot is constructed to locate the the crystal axis. The polar plot for GaAs, taken at tilt angles of 4° and 6° is shown in Fig.4.2. The lines passing through the planar minima points intersect at a point corresponding to $R_1 = 0.2^\circ$ and $R_2(\text{tilt}) = 70^\circ$. The beam is aligned along the $\langle 100 \rangle$ axis by positioning the crystal at these angular coordinates.

4.1.b. Aligned and Random Spectra

The Rutherford Back scattering spectrum for a 1.08 MeV He^+ beam incident along $\langle 100 \rangle$ axis of the as-received silicon single crystal is shown in Fig.4.3a. together with a spectrum taken in an off-axial direction (random spectrum). Similar random and aligned spectra for GaAs(100) crystal are shown in Fig.4.3b. The surface peak in aligned spectra is always present due to the scattering occurring from the top layer. The minimum in the scattering yield is recorded just behind the surface peak.

When the crystal is tilted (but avoiding tilt along a planar channel) around the perfectly aligned direction, the

scattering yield shows an angular dependence as shown in Figure 4.4. This is called as angular scan or angular yield profile. The curve is characterized by the half width $\{ \psi_{1/2} \}$ and the minimum yield $\{ x_{min} \}$. The angular scan is generally taken for the integrated yield over an energy window set just below the surface peak. The maximum in the yield of the angular scan occurs at the shoulders of the angular yield profile. This yield is much larger than the one obtained along a true random direction. The maximum occurs when the beam is oriented at an angle just slightly larger than that required to steer or channel the particles. Under this geometrical configurations the crystal appear more densely packed thus resulting in more close encounters with the lattice atoms giving rise to the wide angle scattering process. As in the case of the minimum yield the half-angle is depth-dependent and is usually determined for energies corresponding to near surface regions.

The angular scans taken for the as received Si and GaAs crystals around the $\langle 100 \rangle$ axial direction are presented in Fig.4 5a & 4.5b. The experimentally determined values of x_{min} , $\psi_{1/2}$ and the thickness of the surface layer(L) for both Si and GaAs are given in Tables 4.1-4.3. The theoretical values of these parameters for the presently employed experimental conditions are calculated below.

Theoretically, the minimum yield $\{ x_{min} \}$, the half-angle $\{ \psi_{1/2} \}$ and the thickness of the surface layer (L) are given by Chu et al., page 237, [13]:

$$x_{min} = Nd\pi(2u^2+a^2) \quad \text{eqn. 4.1}$$

where N is the number of atoms per unit volume,

d is the atomic spacing along the axial direction,

u is the rms thermal vibrational amplitude,

a is the Thomas-Fermi screening radius.

The expression for $\psi_{1/2}$ the half-angle in degrees is given by Feldman et al ,page 235 [13]

$$\psi_{1/2} = 0.8 \text{ FRS } (\xi) \psi_1 \quad \text{eqn. 4.2.}$$

where FRS is the square root of adimensional potential using Moliere's screening function and analytically approximated by the polynomial,

$$\text{FRS}(\xi) = 0.35 e^{-0.3\xi} + 0.55 e^{-1.2\xi} + 0.10 e^{-6.0\xi} \quad \text{eqn 4.3}$$

from Feldman and Mayer,page 96 [14].

$$\xi = 1.2 u / a \quad \text{eqn. 4.4}$$

$$\psi_1 = (2 Z_1 Z_2 e^2 / E d)^{0.5} \quad \text{eqn. 4.5.}$$

where E is the incident energy in MeV,

Z_1 Z_2 the atomic numbers of the projectile and target atoms respectively

The effective number (L) of surface layers contributing to surface peak is given by Chu et al., page 238 [13]:

$$L = (1 + \zeta^2)^{0.5} \quad \text{eqn. 4.5}$$

where $\zeta = 126 u / \{ \psi_{1/2} d \} \quad \text{eqn. 4.6}$

A program to calculate these parameters is given in Appendix 1. The calculated values are also given in Table 4.1 for comparison. It can be seen that the agreement between the experimental and the theoretical values for χ_{min} for both Si and GaAs, and the GaAs surface layers contributing to dechanneling is quite satisfactory. While the higher number of Si surface layers not participating in the

channeling process as compared to the theoretical values can be attributed to the native oxide layers on Si surface. In both the cases the measured value of $\psi_{1/2}$ is much larger (40 % increase for GaAs and 80 % for Si) than of the theoretically calculated values. The increase in the $\psi_{1/2}$ can occur either due to presence of disordered layers (generally oxide layers in case of as received crystals) or due to the tilt moving along a plane.

Table 4 1 A comparison of calculated and measured values of x_{\min}

Target	Direction	Ion	Energy (MeV)	x_{\min}	
				Calculated	Measured
Si	<100>	He	1.09	0.029	0.031
GaAs	<100>	He	1.09	0.038	0.040

Table 4.2 A comparison of calculated and measured values of $\psi_{1/2}$

Target	Direction	Ion	Energy (MeV)	$\psi_{1/2}$	
				Calculated	measured
				(degrees)	
Si	<100>	He	1.09	0.22	0.40
GaAs	<100>	He	1.09	0.24	0.34

Table 4 3 The calculated and measured value of the effective number of surface layers contributing to the surface peak

Target	Direction	Ion	Energy (MeV)	L	
				Calculated	Measured
				(No. of layers)	
Si	<100>	He	1.09	5.79	7.33
GaAs	<100>	He	1.09	4.98	4.85

In summary, the results of channeling measurements performed with the as received Si and GaAs samples show that the channeling set-up has been installed successfully and can now be used for studying various aspects related single crystalline materials viz. ion or laser induced damage, solid phase epitaxy, lattice location of impurities, thin amorphous/disordered layers on a crystalline lattice etc In the following section we present the channeling studies performed on the Si and GaAs crystals subjected to low energy nitrogen ion bombardment using the plasma source ion implantation technique.

4.2 Channeling in plasma immersed Si and GaAs

As mentioned in Chapter I the fabrication of VLSI with sub micron design rules require tools that are capable of highly anisotropic etching for which plasma etching is used almost exclusively because it is a dry process and it can give anisotropic

etching patterns [9] Generally the etching is carried out in CHF_3 , CF_4 etc atmosphere mixed with nitrogen, oxygen or argon to enhance the process [9]. In the course of the etching, the crystals get bombarded with these ions having energies up to 10 keV which degrades the semiconductor device performance. Therefore, the damage which is responsible for this degradation has to be recovered using a suitable process. The problem of the damage induced by low energy ions in Si and GaAs and its recovery has not yet been addressed in detail in the literature. In the following sections the results of channeling investigations of the damage induced by low energy nitrogen ions in Si and GaAs are presented

4.2.1 Damage in Silicon

The channeled spectrum obtained from Si (100) crystal subjected to nitrogen DC arc (2KV) plasma for 6 minutes is shown in Fig.4.6. along with the random spectrum. For comparison, the channeled spectrum of the same crystal before plasma treatment is also shown. The surface position of C, N, O are shown. The peak near to channel number 120 is due to nitrogen embedded in silicon substrate. The area under the peak gives the nitrogen concentration of 7.4×10^{16} atoms/cm². The amount of nitrogen is in reasonable agreement with the one calculated from the plasma irradiation condition (current 50 μ A, the area 6.2 cm², time 6 minutes.). The nitrogen peak is located at an energy of 313.5 keV which is 45 keV less than the expected one. From the calculation of stopping factor [S], the nitrogen peak is at a depth of 750 Å from the surface in Chu et al., page 8 [13]. TRIM calculations show (Fig. 4.7a & 4.7b) that the range of 2 keV

nitrogen ions inside the silicon is 70 \AA . Thus the observed range is 10 times larger. This is because of the channeling of nitrogen ions in silicon. Such enhancement in the ranges are reported in literature for 19 keV Ne^+ in copper crystals by Bierman et al. [30]

The enhanced surface peak and the increase in the dechanneling yield at lower energies are the indications of the damage induced in the near surface region of the Si crystal caused by the displacement of the host atoms from their lattice positions during the passage of nitrogen ions of energies up to 2 keV in the plasma implantation process. The thickness of the damaged surface layer (120 \AA) is obtained from the area under the surface peak. No channeling occurs in this layer. The simulated surface peak is shown by a continuous curve in Fig.4 8. The background arising due to the flat portion of the channeled spectrum has been subtracted for the thickness analysis. The aligned spectra for the implanted crystal lie above the virgin spectrum even at depths below the disordered region. The yield at depths below the disordered region is increased because some of the channeled ions have become dechanneled as a result of the scattering of the particles as they pass through the disordered area. These dechanneled particles may then interact with and be scattered from all the atoms of the crystal. The problem is to separate the two contributions: back scattering of the channeled particles from displaced atoms, and back scattering of dechanneled particles from all the atoms of the crystal.

We calculated the expected value of χ_{min} due to the presence of the disordered layer of 120 \AA (which is equivalent to $5.9 \times 10^{16} \text{ Si atoms / cm}^2$). The probability $P(\psi_{1/2})$ that a particle will be

scattered through angles greater than $\psi_{1/2}$ in a single collision when traversing a film of Nt atoms / cm^2 is given by Chu et al., page 241 [13].

$$P(\psi_{1/2}) = \sigma_D(\psi_{1/2}) * Nt \quad \text{eqn 4.8}$$

$$\sigma_D(\psi_{1/2}) = 3.5 * 10^{-20} Z_2 / E \quad \text{cm}^2 \quad \text{eqn 4.9}$$

where $\sigma_D(\psi_{1/2})$ is the cross section for atoms to deflect particles equal to or greater than the critical angle, E is the incident energy in MeV, Z_2 is the target atomic number. In the present case for 1.09 MeV He^+ ion in Si the value of $P(\psi_{1/2})$ is 3.8 %. That is 3.8 % of the incident particles will be deflected beyond a critical angle. Or in other words the minimum yield should go up by 3.8 % (i.e. total of 6.7 %). But in the present case of Si irradiated sample the measured minimum yield is 23 %, much higher than the expected minimum yield. This enhancement is attributed to the presence of extended defects [31].

The channeling spectra for the annealed cases (for 300°C and 400°C) are shown in Figure 4.9. Figures 4.10a-4.10b shows their simulated spectrums. The area under the surface peaks, after subtracting the area corresponding to the dechanneled portion, is used to calculate the thickness of disordered layer in each case. This thickness and the corresponding number of displaced atoms are given in the Table 4.4.

Table 4.4 The thickness of disorder layers in Si

Sample	Simulated thickness of disordered layer (\AA)	Number of disordered atoms per square cm
Si Implanted	119.73	5.9×10^{16}
Si 300°C Anneal.	93.5	4.6×10^{16}
Si 400°C Anneal.	87	4.3×10^{16}

The calculation of disorder distribution below the surface is quite involved and the necessary program will be developed in future in our laboratory. Such analysis can be performed with the recent version of RUMP (Rutherford Universal Manipulation Program) package which is not available with us at present.

The angular yield profiles for all cases in Si crystal is shown in Figure 4.11. There is an increase in the χ_{\min} value in the case of implanted sample. And one can see how the χ_{\min} value decreases with subsequent annealing temperatures.

Table 4.5 The χ_{\min} and $\psi_{1/2}$ values measured for Si

	χ_{\min}	$\psi_{1/2}$ (in degrees)
Si Implanted	0.23	0.20
Si 300°C Anneal.	0.21	0.52

4 2 2 Damage in GaAs

The channeled spectrum of 2 keV nitrogen implanted GaAs (100) is shown in Fig 4 12 and the simulated surface peak is shown in Fig.4 13. The surface peak of the implanted is larger compared to the surface peak of the virgin aligned as expected. The analysis has been done as in case of Si for the χ_{min} , $\psi_{1/2}$ etc and the results are given in the Table 4.7. In this case the nitrogen peak is not clearly visible due to the large background arising from scattering of Ga and As atoms.

We calculated the expected value of χ_{min} due to the presence of the disordered layer of 66 Å^o (which is equivalent to 3×10^{16} GaAs atoms / cm²) as 7 % while the measured χ_{min} value is 9.3 %. This indicates that the amount of extended defects created below the surface in case of GaAs is much less than in silicon.

The channeling spectra for the annealed cases (for 300°C and 400°C) are shown in Figure 4.14. Figures 4.15a-4.15b. shows their simulated spectra. By finding out the area under the surface peaks after subtracting the area corresponding to the dechanneled portion we estimate the total number of disordered atoms in each case. The number of atoms displaced from regular lattice sites which are summarized on the Table 4.6

Table 4.6 The thickness of the disorder layer in GaAs

Sample	Simulated thickness	Number of disordered
--------	---------------------	----------------------

of disordered layer atoms per square cm.
(A°)

GaAs Implanted	66.4	$3.05 * 10^{16}$
GaAs 300°C Anneal.	45.5	$2.09 * 10^{16}$
GaAs 400°C Anneal.	41	$1.86 * 10^{16}$

The angular yield profiles for all cases in GaAs crystal are shown in Figure 4.16. We can see $\chi(\text{min.})$ decreases with the annealing temperatures.

Table 4.7 The χ_{min} and $\psi_{1/2}$ values obtained for GaAs

	χ_{min}	$\psi_{1/2}$ (in degrees)
GaAs as-received	0.04	0.38
GaAs Implanted	0.093	0.48
GaAs 300°C Anneal.	0.090	0.55
GaAs 400°C Anneal.	0.07	0.59

4.3 Four-Point Probe Resistivity Results.

The four-point probe resistivity measurement results for virgin, implanted and annealed samples are given in Table 4.8.

Table 4.8 Four-Point Probe Resistivity Results in Si and GaAs

Sample	Sheet Resistivity (Ω / \square)
Si Virgin	1.0
Si 2 keV Nitrogen Implanted	Very high (Not in measurable range)
Si implanted and 300°C annealed	(same)
Si implanted and 400°C annealed	1.1
GaAs Virgin	1.4
GaAs 2 keV Nitrogen Implanted	Very high (Not in measurable range)
GaAs Implanted and 300°C annealed	(same)
GaAs Implanted and 400°C annealed	2.1

The sheet resistivity is too high to be measured for the implanted samples and complete electrical recovery occurs after the 400°C anneal. The resistivity of the damaged samples is not measurable since the dopant atoms are either removed from the substitutional sites or get deactivated due to presence of disorder. But the channeling results show that there is still some disorder even after the 400°C anneal.

There are two possible reasons for this difference. First, it is possible that the fraction of displaced dopant atoms restored to their substitutional sites saturates earlier than the host displaced atoms. The second reason can be attributed to the sensitivity of

carrier delocalization to the presence of disorder in the host material. The typical Bohr radius for shallow dopants in semiconductors is of the order of 100\AA i.e. the carrier samples the host over several tens of lattice spacings. Presence of disorder in the vicinity of the dopant atoms (within the sample volume corresponding to Bohr radius) would lead to carrier localization even if the dopant is at its substitutional site. With annealing the probability of occurrence of disorder in the vicinity of dopant atoms can become small even if the host has not fully recovered. Since similar results are obtained for two completely different systems viz Si:B and GaAs:Zn, the reason for difference between channeling and electrical activation cannot be attributed to any special characteristics of either the dopant or the host. Hence the later reasoning seems more attractive.

4.4.The recovery of surface damage.

Figure 4.17a gives the percentage of disorder remaining in the Si crystals after each annealing. The driving force for the regrowth of an amorphized layer is very large and disordered atoms are swept into the lattice sites even for peak concentrations which are larger than the solubility at the regrowth temperature. The situation is different for low mass low dose implantation. In our case we observed monotonous decrease in the fraction of disordered host atoms with increasing annealing temperature.

Figure 4.17b gives the percent of disorder remaining in the GaAs crystals after each annealing. We can observe the decrease in the

fraction of disordered host atoms with increasing annealing temperature.

The number of displaced atoms after plasma irradiation is approximately twice of that in GaAs, due to the fact that Ga and As atoms are heavier compared to Si. RBS analysis of channeled spectra shows that the range of nitrogen ions in Si is more than the range predicted by TRIM . This is probably due to channeling of the nitrogen ions into the crystal In GaAs since the nitrogen peak was not seen There was significant increase in χ_{min} value in case of implanted silicon as compared to GaAs. In both cases extended defects are created. The recovery of damage with annealing was similar for both Si and GaAs. In both cases of GaAs and Si the damage as seen by channeling is partial even after 400°C anneal whereas both recover as far as dopants are concerned

SUMMARY AND CONCLUSIONS

Ion channeling is a remarkably powerful analytical technique which provides direct quantitative information about the lattice disorder and the location of impurity atoms in a crystalline matrix. Such basic studies using channeling measurements had been the backbone of the many developments in semiconductor device technology since early 1970s. Simultaneously, channeling as materials analysis technique also grew in terms of its wide range of applicability and the variety of defect related questions which it could address. The development of a new process, which involves surface modification of crystalline samples viz. epitaxy, plasma etching etc., depends on the information obtained from channeling measurements. The channeling results help in understanding the physics and most importantly in standardizing the process. This work was primarily undertaken to install and test a modern channeling facility in our institute. Further, the study of low energy ion induced damage produced during the plasma etching process was undertaken using this facility.

A precision Sample Manipulator having stepper motor controlled rotations around three mutually perpendicular axes and three translational movements along the three axes (from High Voltage Engineering Europa, Netherlands) forms the heart of the system. A suitable vacuum chamber has been fabricated with arrangements for sample mounting, secondary electron suppression and detector holder. The He^+ beam ion of size 2 mm x 2 mm is obtained at the intersection of the three mutually perpendicular rotation axes of the manipulator. The beam divergence has been kept $< 0.06^\circ$ using beam defining slits of

2 mm x 2 mm size placed at a distance of 2 m apart along the beam line. The test experiments have been performed using p-type Si (100) and p-type GaAs (100) single crystals. The parameters χ_{\min} , $\psi_{1/2}$ and the thickness of layers (L) contributing to surface peak were measured.

Low energy nitrogen irradiation was done using a DC plasma immersed ion implantation set-up using arc voltage of 2 KV. The damage induced in Si and GaAs due to this process has been studied by measuring the different parameters mentioned above. The effect of iso-chronal annealing has been studied to understand the recovery of the damage in conjunction with four-point probe resistivity measurements.

The main achievements and conclusions of this thesis work are listed below

- 1) The Channeling set-up has been installed and tested using Si and GaAs as-received crystals.
- 2). The aligned spectra taken along <100> axis gives the values of $\chi_{\min} = 3.1\%$, $\psi_{1/2} = 0.4^\circ$ and $L = 7.33$ for Si and $\chi_{\min} = 4\%$, $\psi_{1/2} = 0.34^\circ$ and $L = 4.85$ for GaAs. The values are in reasonable agreement with the theoretically calculated ones.
- 3) The channeled spectra for low energy nitrogen plasma irradiated Si and GaAs samples give disordered layers of thickness 120°\AA and 66°\AA respectively. The observed χ_{\min} values are 23 % for Si and 9.3 % for GaAs. For Si this value is significantly larger than the calculated value of 6.7 % indicating the presence of extended defects. However, in the case of GaAs this difference is only 2% implying much smaller amount of extended defects below the surface.

4) The nitrogen distribution is clearly visible in case channeled spectrum taken for irradiated Si while for GaAs it is not visible due to the large background. RBS analysis of the nitrogen peak for Si spectrum gives an irradiation dose of 7×10^{16} atoms / cm^2 . The order of magnitude agrees with the expected dose calculated from the plasma irradiation parameters.

5). The nitrogen peak is located at a depth of 800°\AA which is about 10 times deeper than the range calculated using TRIM. This is attributed to the channeling of nitrogen ions in Si crystal

6) The reduction disorder of near surface region is seen as a function of annealing temperature. However, the exact dependence and the calculation of activation energy for the recovery process require annealing at higher temperatures. The channeling parameters (χ_{min} etc.) showed systematic improvement in their values after iso-chronal annealing. However complete damage recovery has not taken place even after 400°C anneal. On the other hand the sheet-resistivity which became unmeasurable after nitrogen irradiation gets restored to its original value after annealing at 400°C .

REFERENCES

- 1 Ziegler J F., in Ion Implantation Science and Technology,
Academic Press NY (1984).
- 2 Tuszewski M., Scheur J. T , Campbell I. H., and Laurich B. K.,
Journal of Vac Sci and Technol , B12 (2), (1994) 973.
- 3 Robinson M. T. and Oen O S., Phys. Rev., 132, (1963) 2385
4. Gemmel D. S., Rev. Mod Phys., 46, N.1, (1974) 129.
5. Morgan D. V., in Channeling, John Wiley and Sons (1973)
- 6 Narayan J. and Tan T Y., in Defcts in Semiconductors, North
Holland (1981).
- 7 Sze S. M., in V.L.S.I Technology, Mc Graw Hill NY (1983).
- 8 Conrad J. R., Radtke J. L., Dodd R. A., Worzala F. and Tran N.
C , J. Appl. Phys , 62, (1987) 4591
- 9 Li Y. X., French P. J. and Wolffenbuttel R. F , Journal of
Vac Sci and Technol., B13(5), (1995) 2008.
10. Hughes W. C., Rowland W H., Johnson M. A. L. Jr , Shizuo Fujitha,
Cook. J. W. Jr. and Schetzinaa J. F., Journal of Vac Sci. and
Tech., B 13(4) (1995).
- 11 Banerjee N., Ph D. Thesis, IIT Kanpur, India (1993)
12. Choudhuri P., in Ion Beam Mixing Study of Si-Ge System, MTech.
Thesis, IIT Kanpur, India (1993).
- 13 Chu W. K , Mayer J. W. and Nicolet M A., in Backscattering
Spectrometry, Academic Press NY (1978).
14. Feldman L. C. and Mayer J. W. in Fundamentals of Surface and Thin
Film Analysis, North-Holland, (1986).
15. Doolittle L R., Nucl. Instr. Meth., B9(1985) 334.

16. Biersack J. P., Haggmark L., Nucl Instr Meth , (1980) 174.
17. Ziegler J. F , in The Stopping of Ions in Solids, Pergamon Press, NY (1985).
- 18 Feldman L. C. and Appleton B. R , Phys Rev., B 8, (1973) 935.
- 19 Appleton B. R , Datz S., Moak C. D. and Robinson M. t , Phys. Rev., B 4, (1971) 1452.
20. Barrett J. H., Phys. Rev , B 3, (1971) 1527.
21. Ramakrishnan K. in Temp. Dependence of Ion Beam Mixing in Si-Ge, MTech Thesis, IIT Kanpur, India (1994).
22. Som T., Dhar S. and Kulkarni V. N , Proceed of National Symposium on Plasma Sciences, IIT Kanpur India (1995).
23. Qin S., Chan C. and McGruer N. E., Plasma Sources Sci. Technol., 1 , (1992).
24. Pico C. A., Libberman M. A. and Cheung N W., J. Electron. Mater., 21, (1992) 75.
- 25 Tends J., Donnelly I J., Kenney M J. and Pollack J. T. A , Appl. Phys. Let., 53, (1988) 2143
- 26 J. N. Matossian, J. J. Vajo, J. A. Wysocki and M E. Ballon., Surf. Coat. Techol , 62, (1993) 595.
27. Conrad J. R., Radtke J. L., Dodd R. A., Worzala F. and Tran N C , J. Appl. Phys., 62, (1987) 4591.
- 28 Mayer J. W. and Rimini E , in Ion beam Hand Book for Material Analysis., Academic Press, NY (1977).
29. Dieter K Schroder in Semiconductor Materials and Device Characterization., John Wiley & Sons, Inc. (1990).
- 30 Bierman, D J. and Van Vliet, D. Physica, 57, (1972) 221.

- 31 Foti G., Csepregi L , Kennedy E F., Pronko P. P. and Mayer J. W , Phys. Lett , 64A, (1977) 265.
31. Balaji S., in Fabrication of a Scattering Chamber, Experimental Project, IIT Kanpur India (1995)

APPENDIX 1

```
program cha (input,output ),
```

```
{This program calculates the values of chi( min)
and psi(1/2) in axial channeling }
```

```
VAR
```

```
  Z1,Z2                :integer;
  M2,E,D0,D,THETA,T,N,a,aa :real;
  u,b,u1,y,x,f,p,L :real,
  psi1,psi,chin:real;
```

```
  {These constants and variables are defined at the end of the progr
  function deb(x:real).real;
  {This is to evaluate the Debye Function
  values for various values of x}
```

```
VAR
```

```
  i          :integer,
  t,h,sum .real;
```

```
BEGIN
```

```
  h      := x/20;
  t      := 0.000001,
  sum    := 0.5*t/(exp(t)-1);
  FOR i:=2 TO 19 DO
      BEGIN
          t :=t+h;
          sum:=sum+ t / (exp(t)-1);
      END;
  sum:=sum + (0.50* x) / (exp(x)-1);
  sum:= sum*( 1/20 );
  deb := sum,
  END;
```

```
BEGIN
```

```
  writeln (' Z1 atomic no of incident ion= ');
  readln (Z1);
  writeln ( 'Z2 atomic no.of target crystal = ');
  readln (Z2);
  writeln ('M2 atomic mass of target crystal = ');
```

```

readln (M2),
writeln (' E Energy of the incident ions ( in mev ) = '),
readln (E);
writeln ('D0 Lattice constant of crystal (in angstroms) = '),
readln (D0);
writeln (' D atomic spacing along axial direction (in angstroms)
readln(D);
writeln ( 'THETA Debye Temperature (in kelvin) = ');
readln (THETA);
writeln ( 'T crystal temperature (in kelwin ) = ');
readln (T);
writeln ( in (in atoms per cubic angstroms)= ');
readln (N);
x :=THETA/T;
aa :=sort(Z1)+sort(Z2);
a :=0.4685 / (exp(0.667*ln(aa))),
u.= deb(x)/x;
b:=( u+0.25)/ (M2*THETA);
u1:=12.1*sort(b);
y .:=1.2*u1/a;
f := 0.35*exp (-0.3*y) +0.55 * exp (-1.2 *y)+0.1 *exp(-6*y);
{This equation is used in computer simulations for Moliere approxim
to the Thomas-Fermi screening function }
psi1:=0.307 * sqrt (Z1*Z2/(E*D));
psi:=0.8*f*psi1;
p :=126*u1/(psi*D),
chimin:=18.8*N*D*sqr(U1);
L :=sqrt (1+p*p),
writeln ('Thomas-Fermi screening radius in angstroms(a) =',a);
writeln ('Normalized distance of closest approach =',y);
writeln (' The value of 1-Dimensional rms thermal ');
writeln (' vibrational amplitude U1 = ',u1);
writeln (' The value of the Thomas-Fermi screening function(Frs) =
writeln ('characteristic angle psi(1) = ',psi1 );
writeln (' half-width for axial channeling psi(1/2) = ' , psi);
writeln ('the minimum yield, chi(min) = ' , chimin);
writeln ('effective no. of surface layer = ',L);

```

END.

Sample output file.

Z1 atomic no. of incident ion=
Z2 atomic no.of target crystal =
M2 atomic mass of target crystal =
E Energy of the incident ions (in mev) =
D0 Lattice constant of crystal (in angstroms) =
D atomic spacing along axial direction (in angstroms) =
THETA Debye Temperature (in kelvin) =
T crystal temperature (in kelwin) =
N (in atoms per cubic angstroms)=
Thomas-Fermi screening radius in angstroms (a) = 1.56893E-01
Normalized distance of closest approach = 5 77277E-01
The value of 1-Dimensional rms thermal
vibrational amplitude U1 = 7.54757E-02
The value of the Thomas-Fermi screening function (Frs) = 5.72590E-01
characteristic angle psi(1) = 6.69587E-01
half-width for axial channeling psi(1/2) = 3 06719E-01
the minimum yield, chi(min) = 2 89158E-02
effective no of surface layer (L) = 5.82816E+00

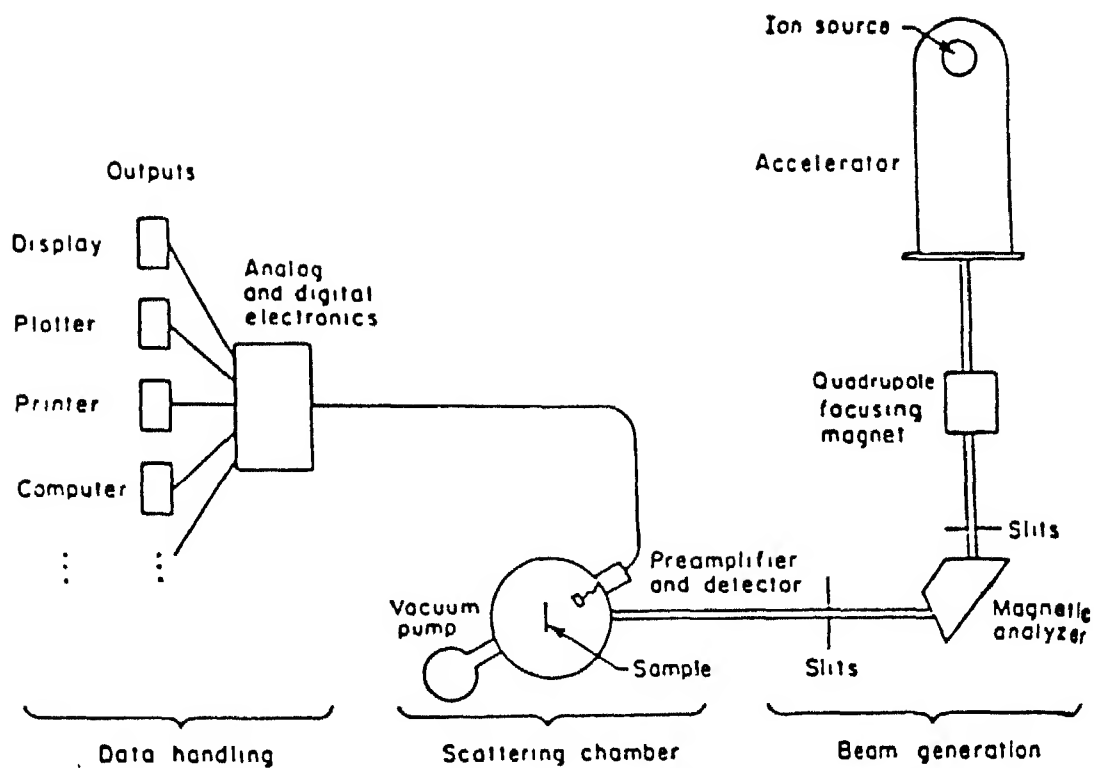


FIG 2.1 Schematic diagram of a typical backscattering spectrometry system in use today.

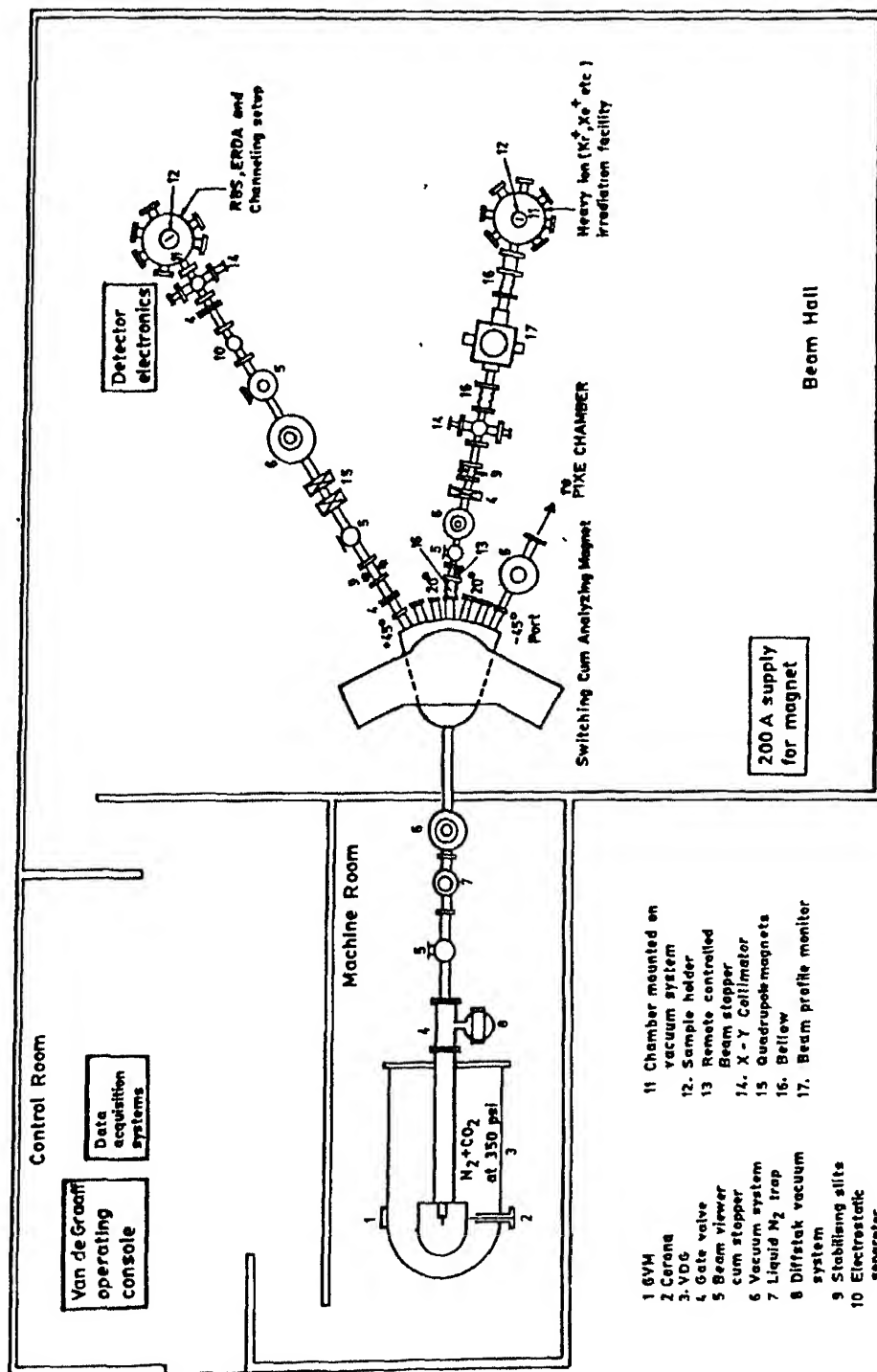


Fig. 2.2. LAYOUT OF ACCELERATOR SET UP.

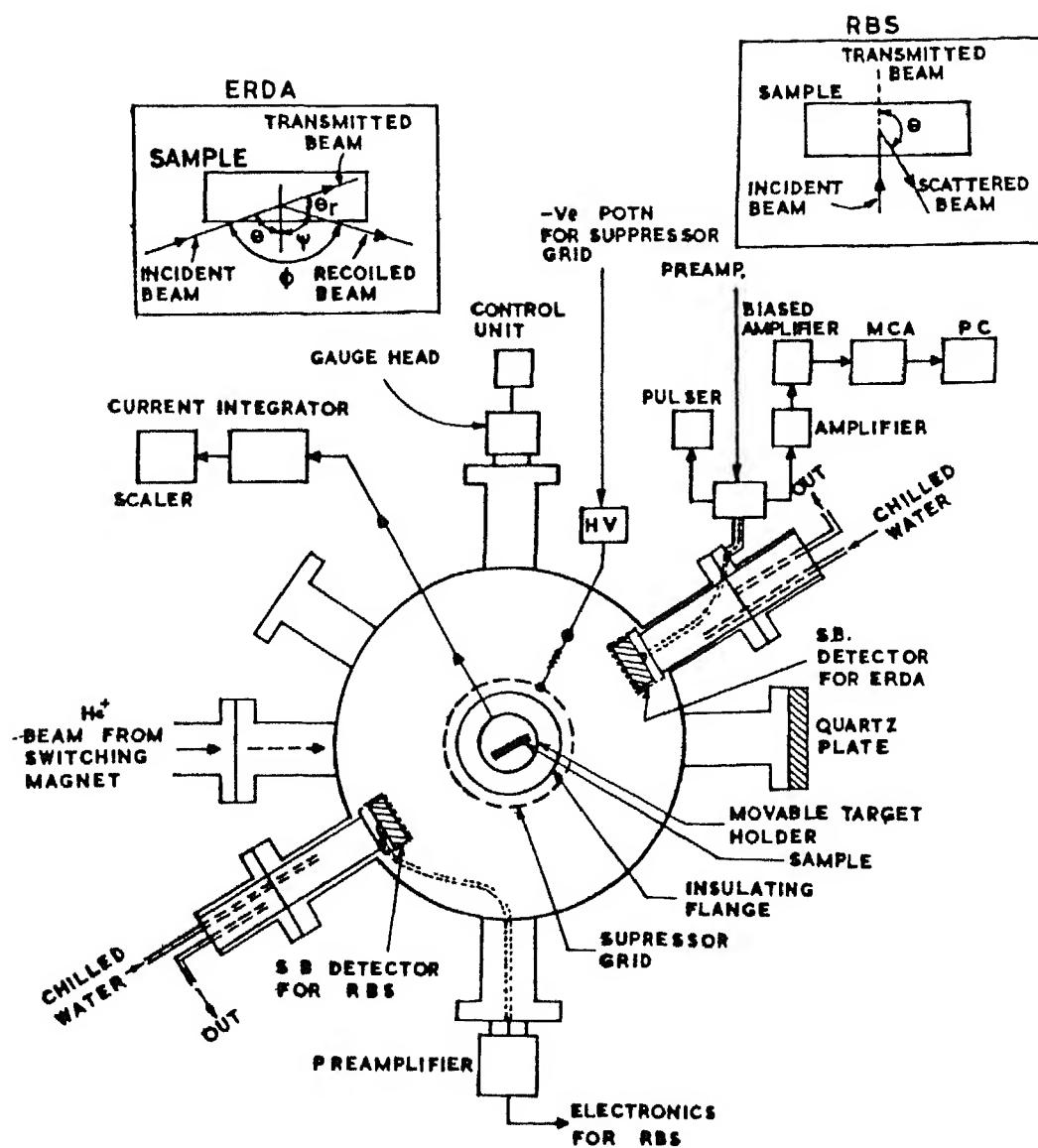


Fig. 2.3. BLOCK DIAGRAM OF THE CHAMBER AND ASSOCIATED ELECTRONICS FOR RBS AND ERDA MEASUREMENTS.

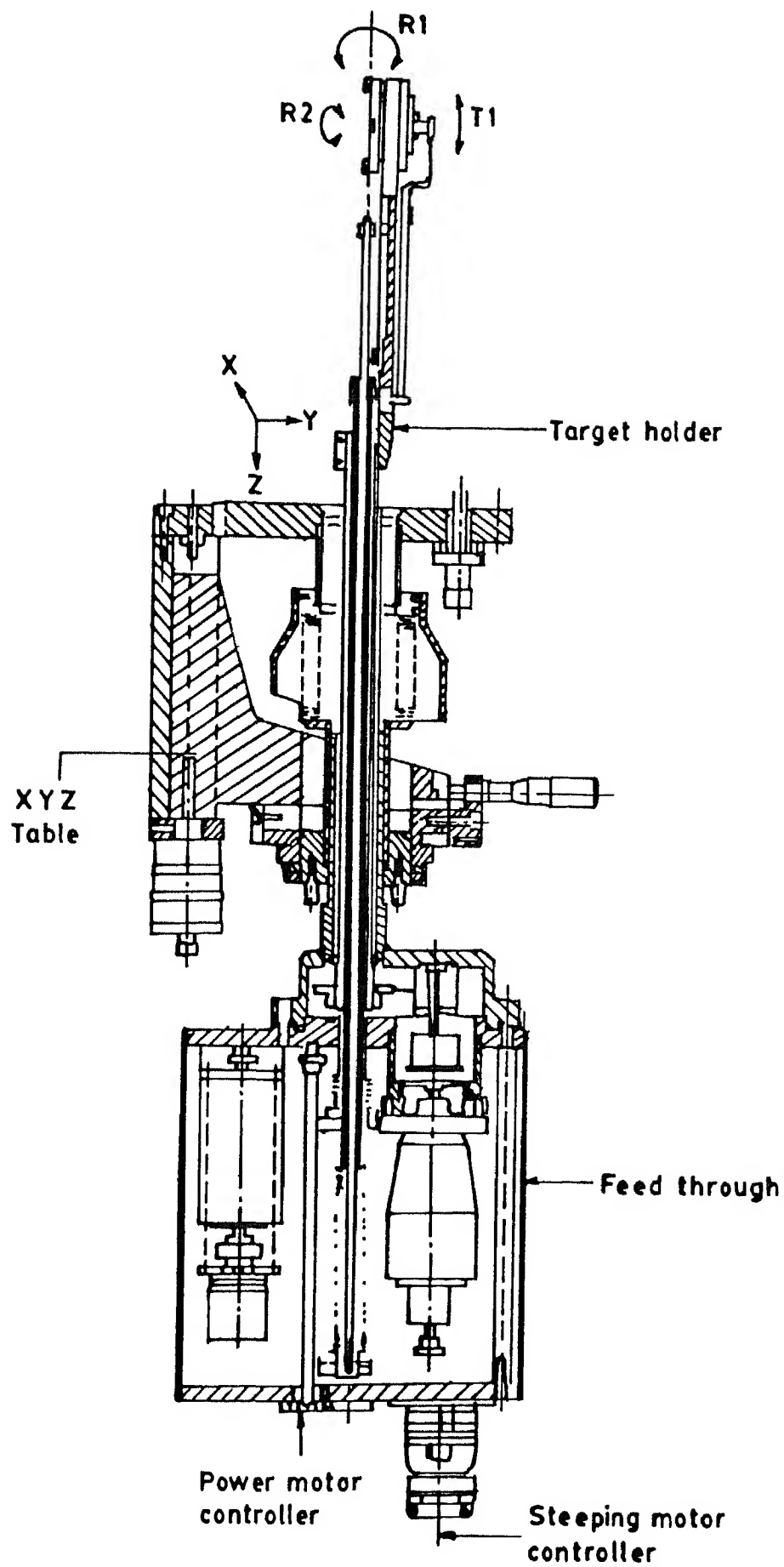


Fig. 3.1. UHV SAMPLE MANIPULATOR

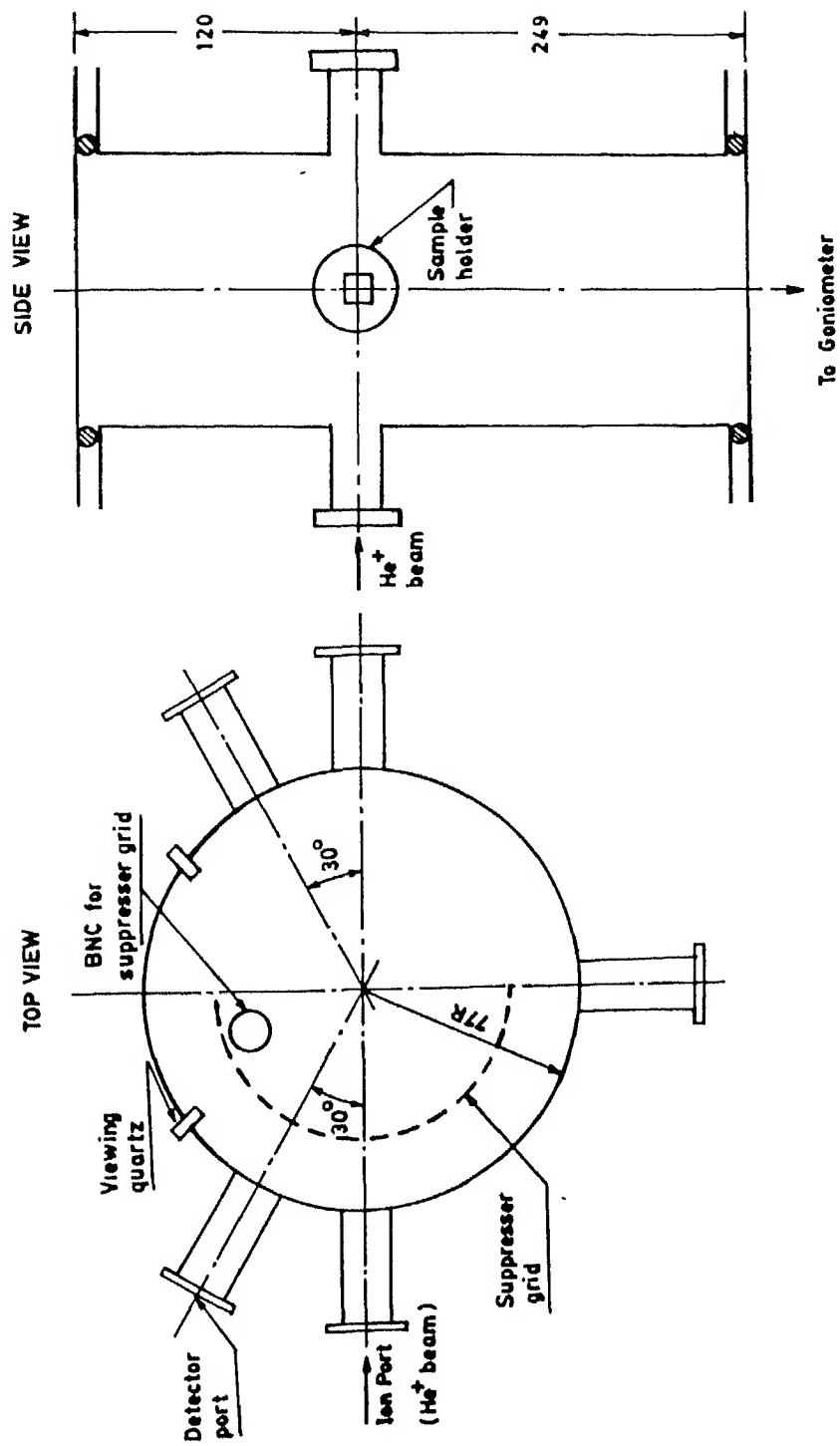


FIG. 3.2 SCHEMATIC DIAGRAM OF CHANNELING PORT

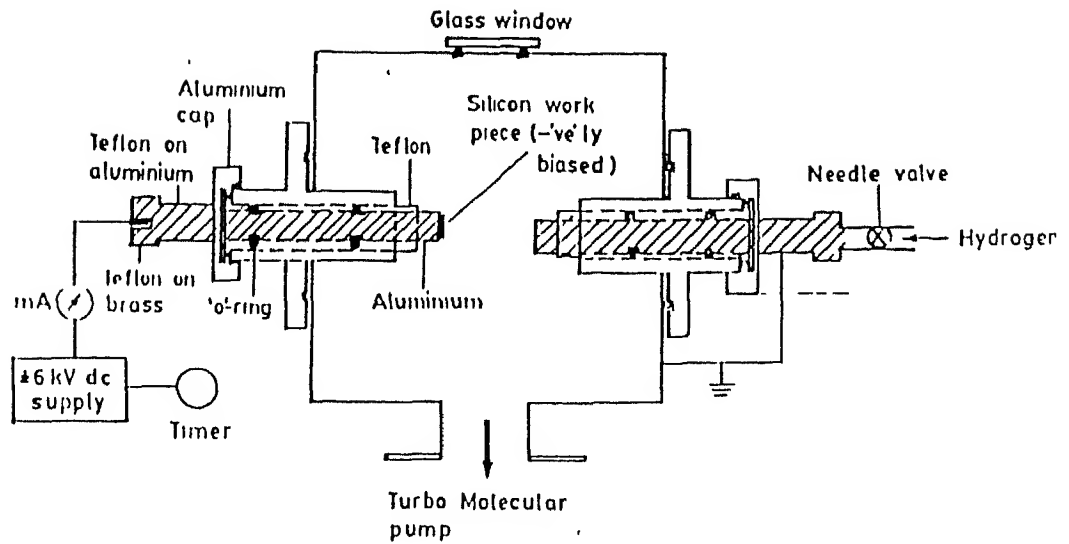


Fig. 3.3. DC Plasma Immersed Ion Implantation Set up.

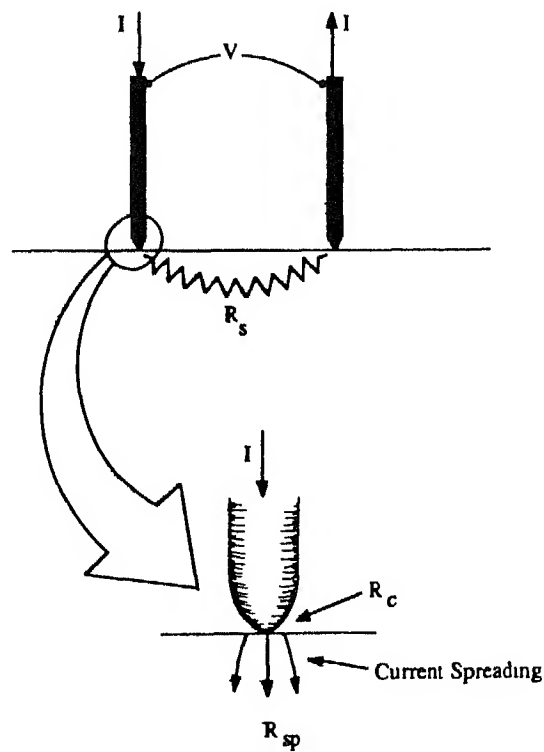


Fig. 3.4.

A two-point probe showing the contact resistance R_c the spreading resistance R_{sp} and the semiconductor resistance R_s .

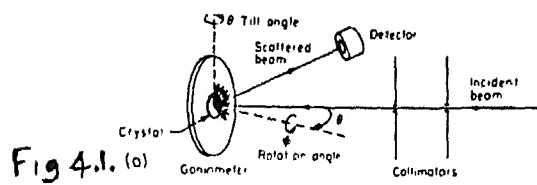


Fig. 4.1a. Schematic drawing of the scattering geometry in channeling experiments.

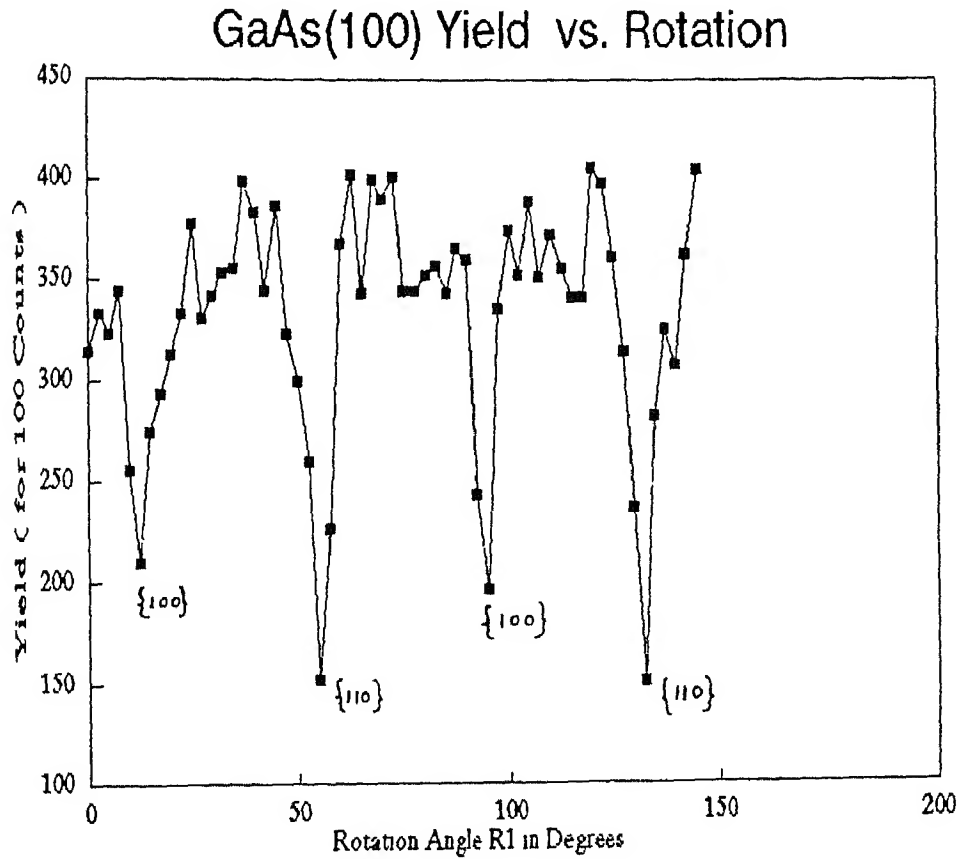


Fig. 4.1b. Scattering yield from the surface of the GaAs (100) crystal as a function of rotation angle R1.

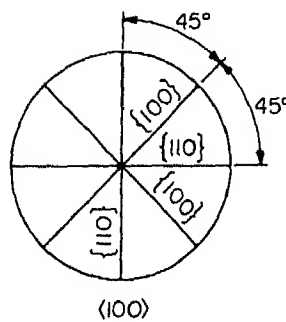


Fig. 4.1c. Orientation of major planes around the $\langle 100 \rangle$ in cubic crystals.

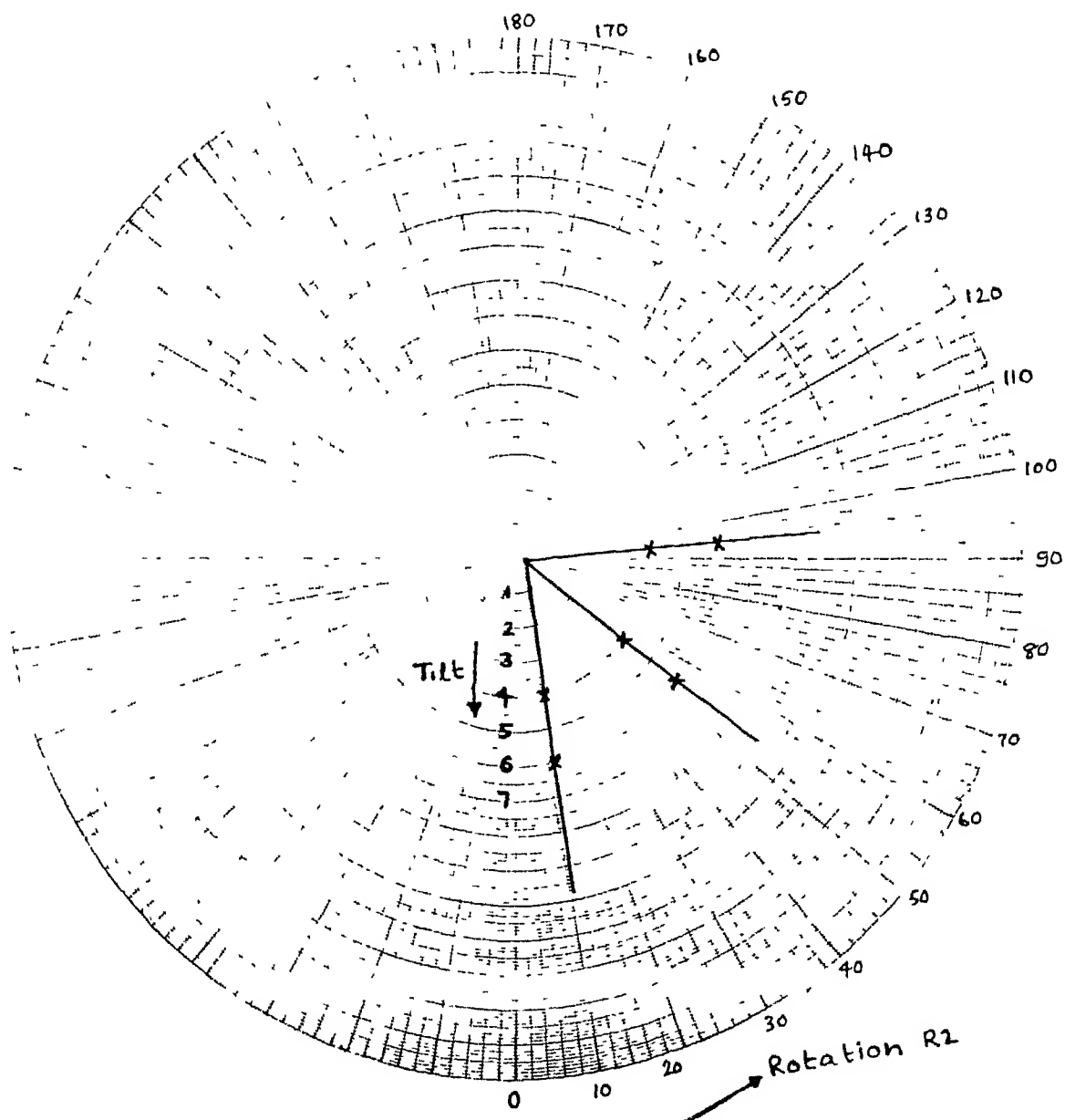


Fig. 4.2. Location of the planar minima on polar coordinates for tilts (R1) 4° and 6° in GaAs (100).

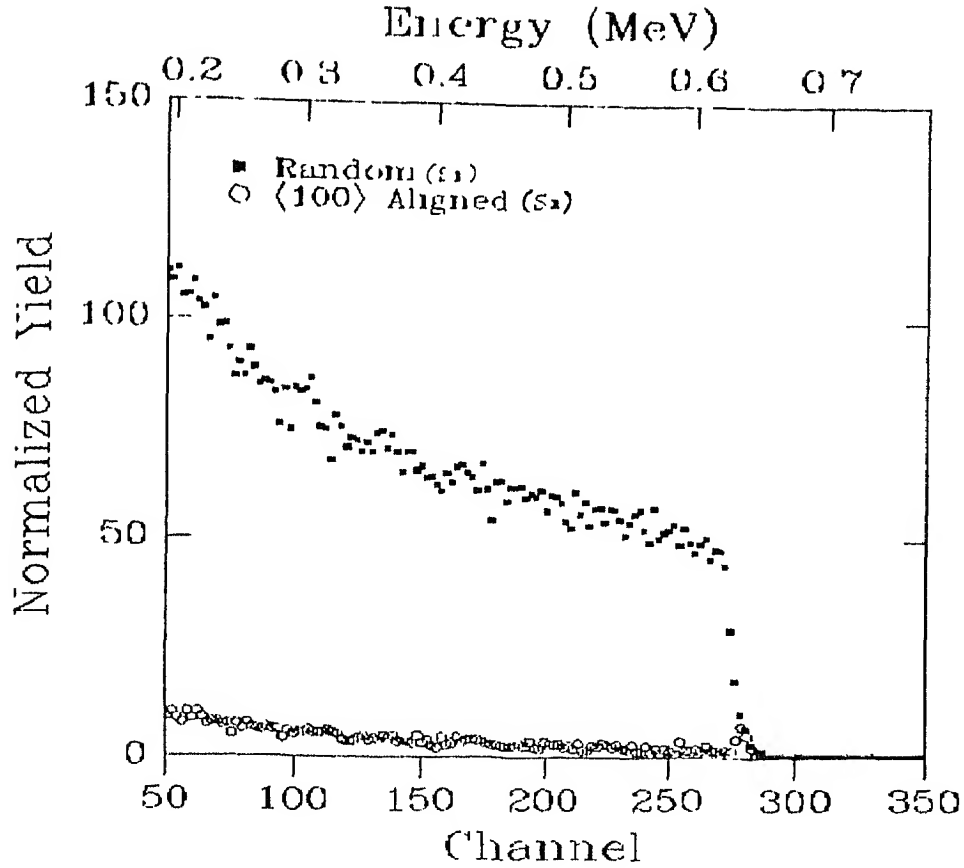


Fig 4 3a. Aligned and random RBS spectra of as-received Si (100).

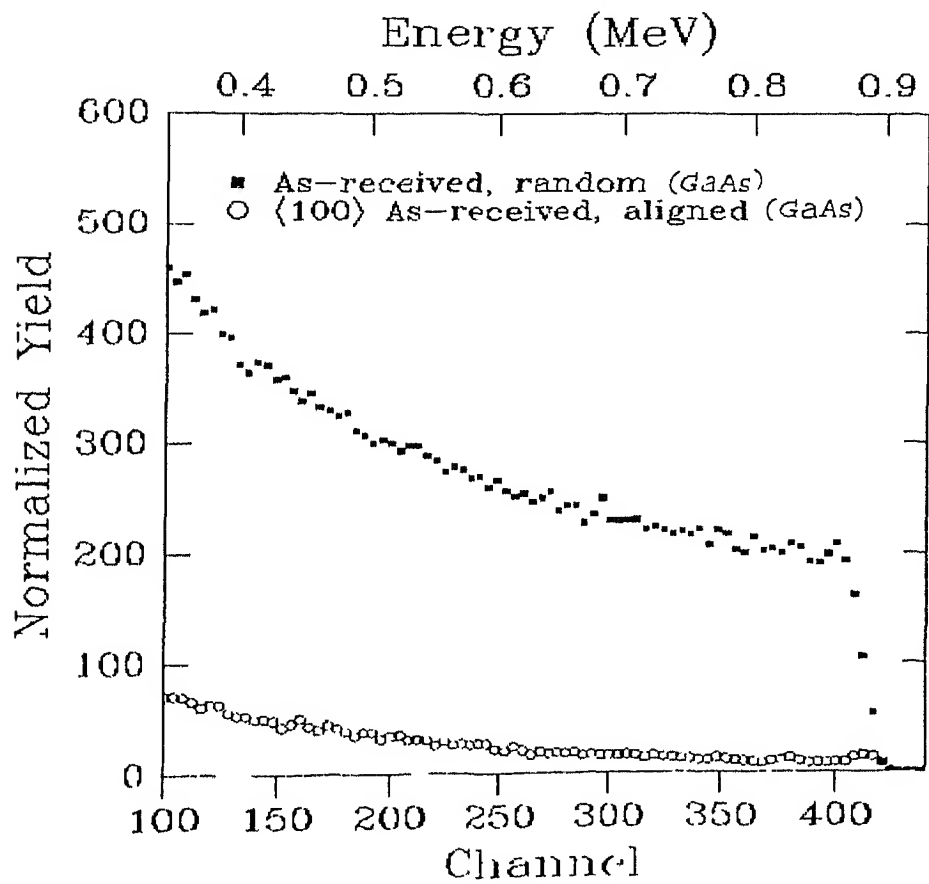


Fig. 4.3b Aligned and random RBS spectra of as-received GaAs (100).

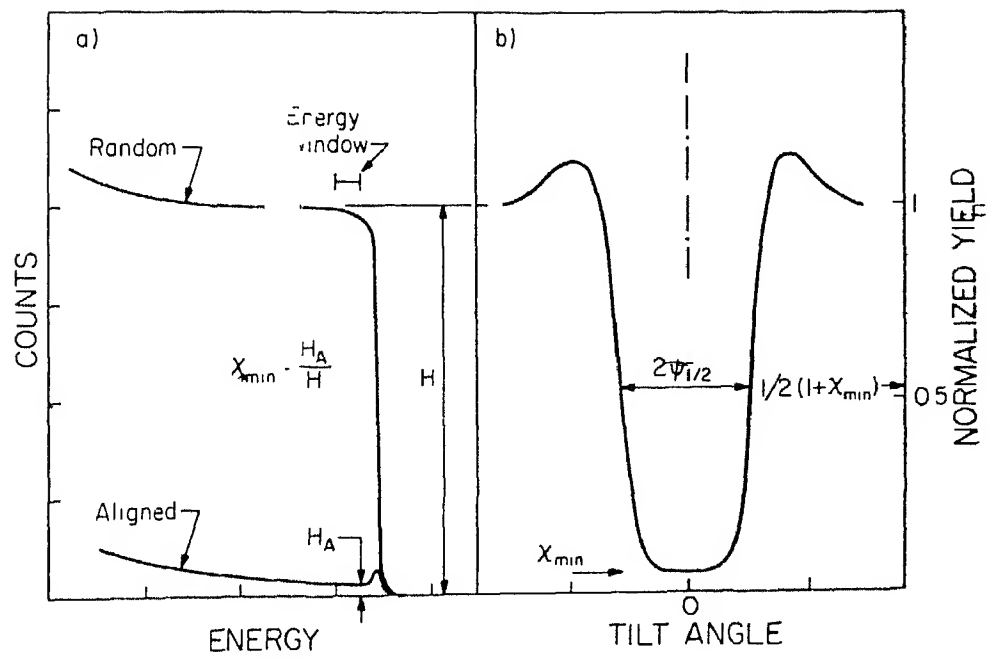


Figure 4.4 Backscattering spectra and angular yield profile.

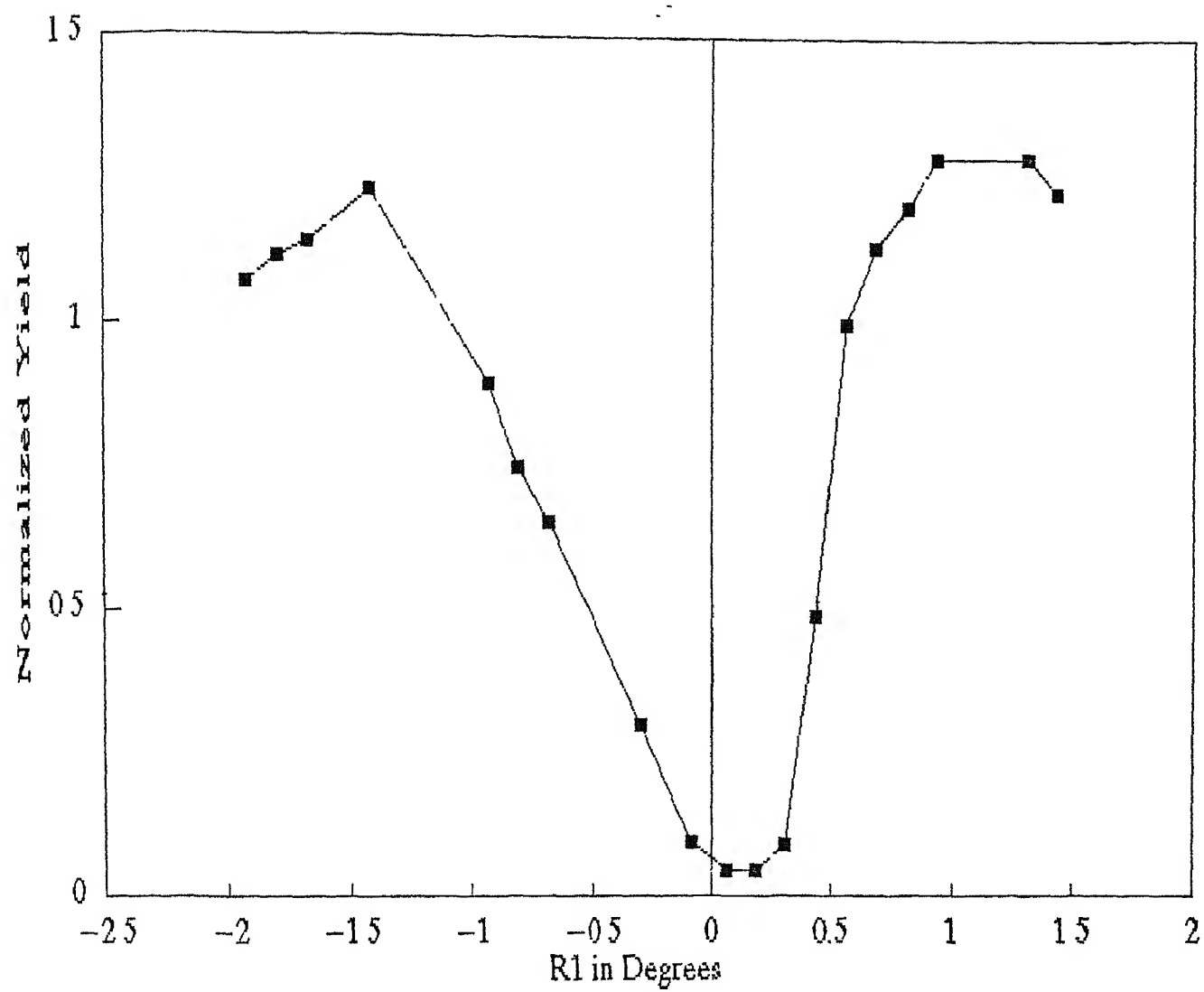


Fig. 4.5a. Angular yield profile for as-received Si (100).

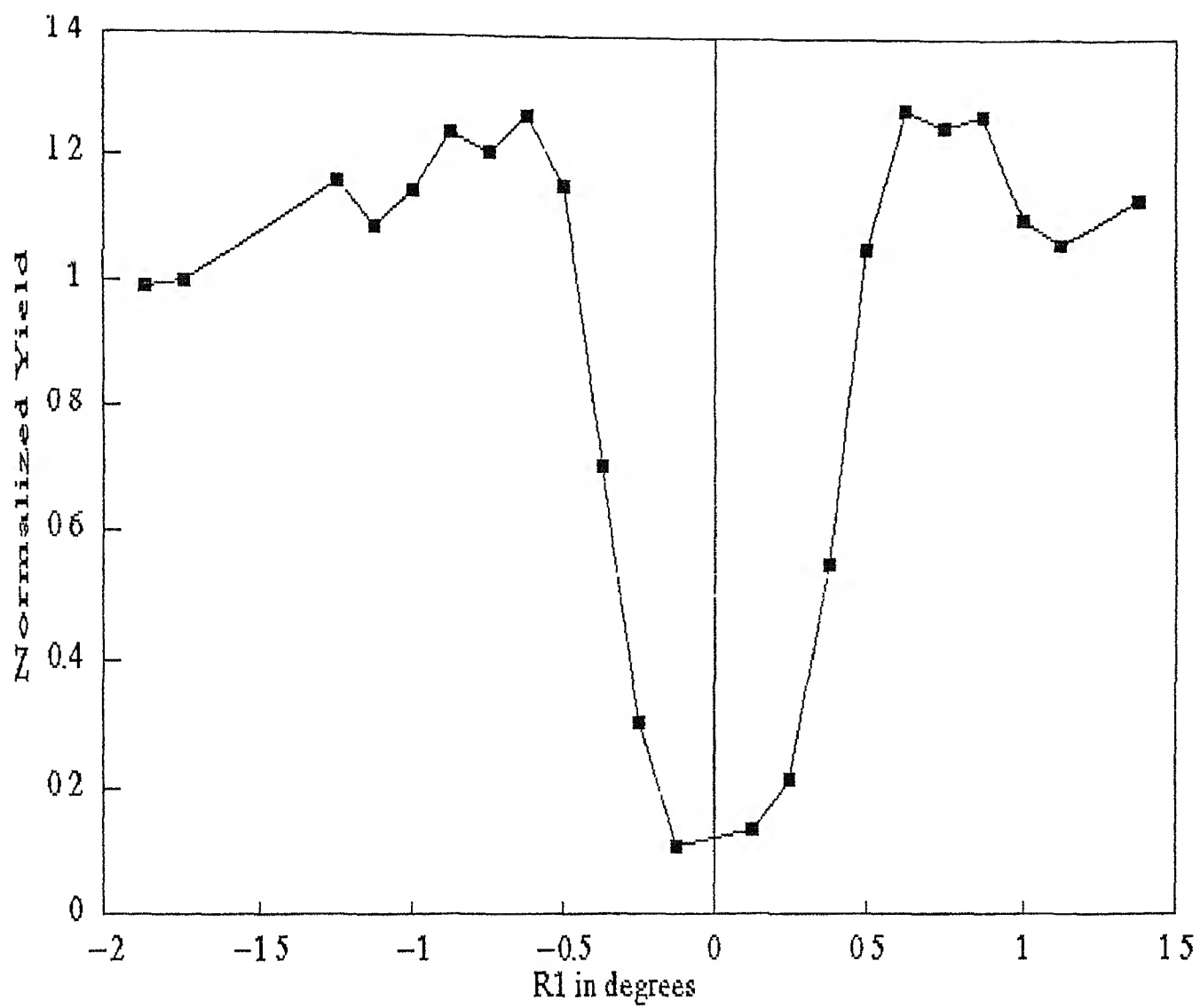


Fig. 4.5b. Angular yield profile for as-received GaAs (100).

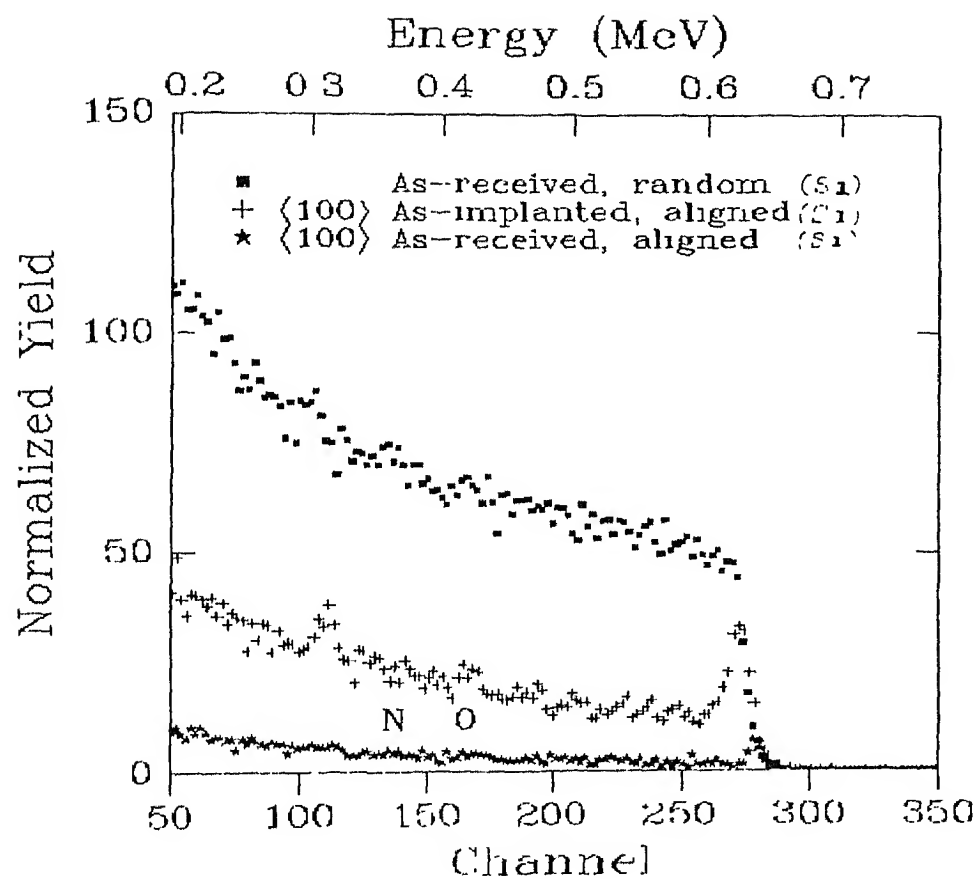


Fig. 4.6 Aligned and Random spectra for 2 keV nitrogen implanted Si.

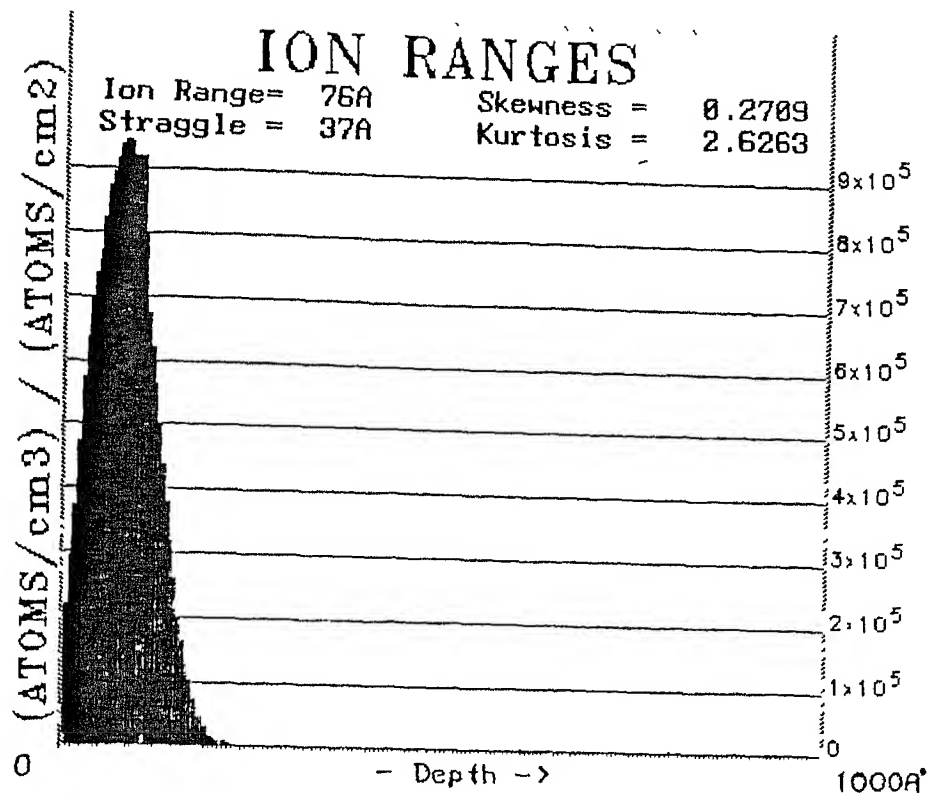


Fig. 4. 7a. TRIM calculations showing the range of 2 KeV nitrogen ions in Si (100).

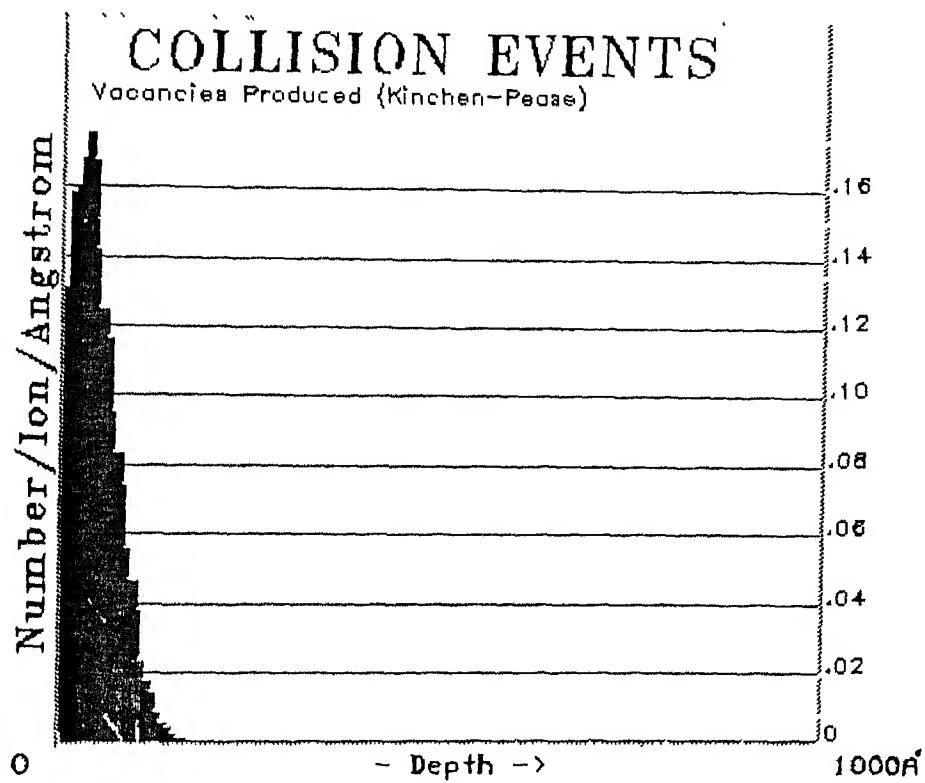


Fig. 4. 7b. TRIM calculations showing the distribution of vacancies produced in Si (100) by 2 KeV nitrogen.

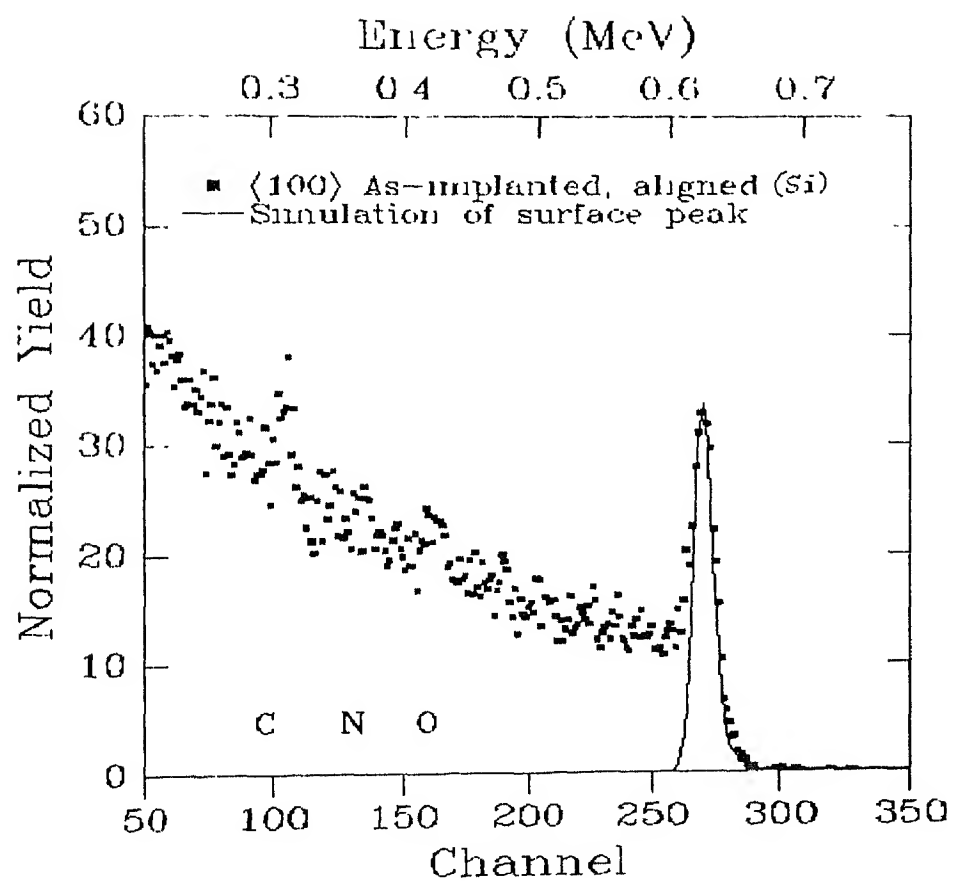


Fig. 4.8. Simulated surface peak for aligned RBS spectrum of 2 KeV nitrogen irradiated Si.

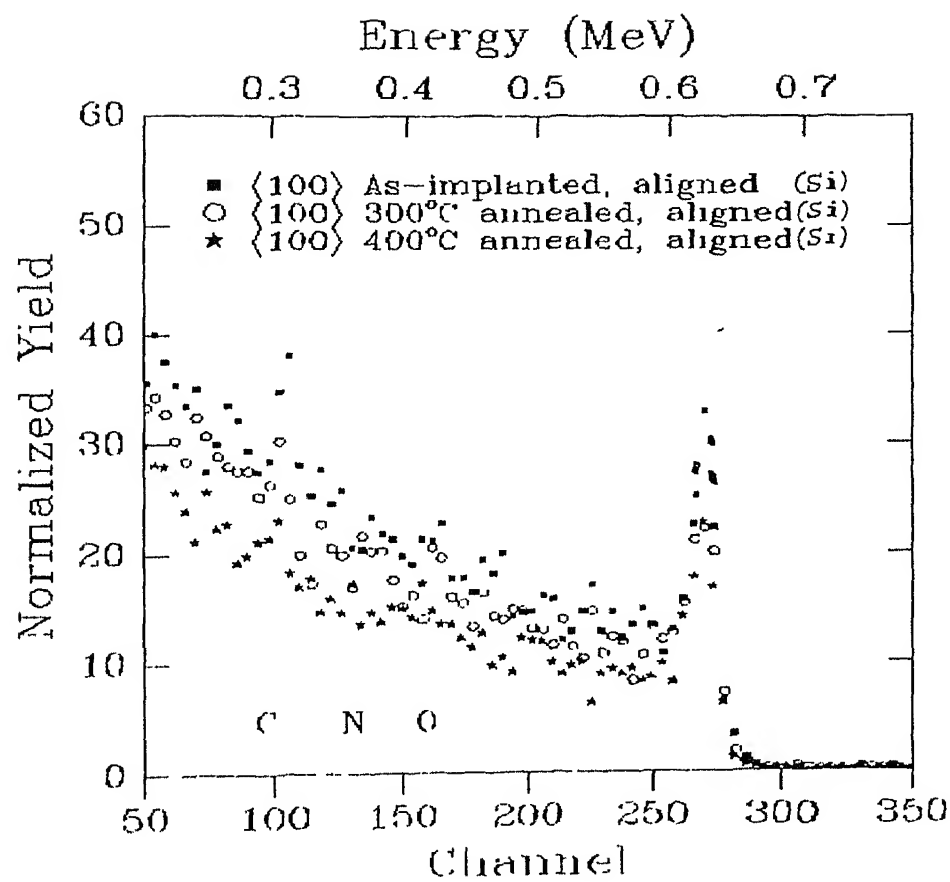


Fig. 4.9. Aligned RBS spectra for the 300°C and 400°C annealed Si(100).

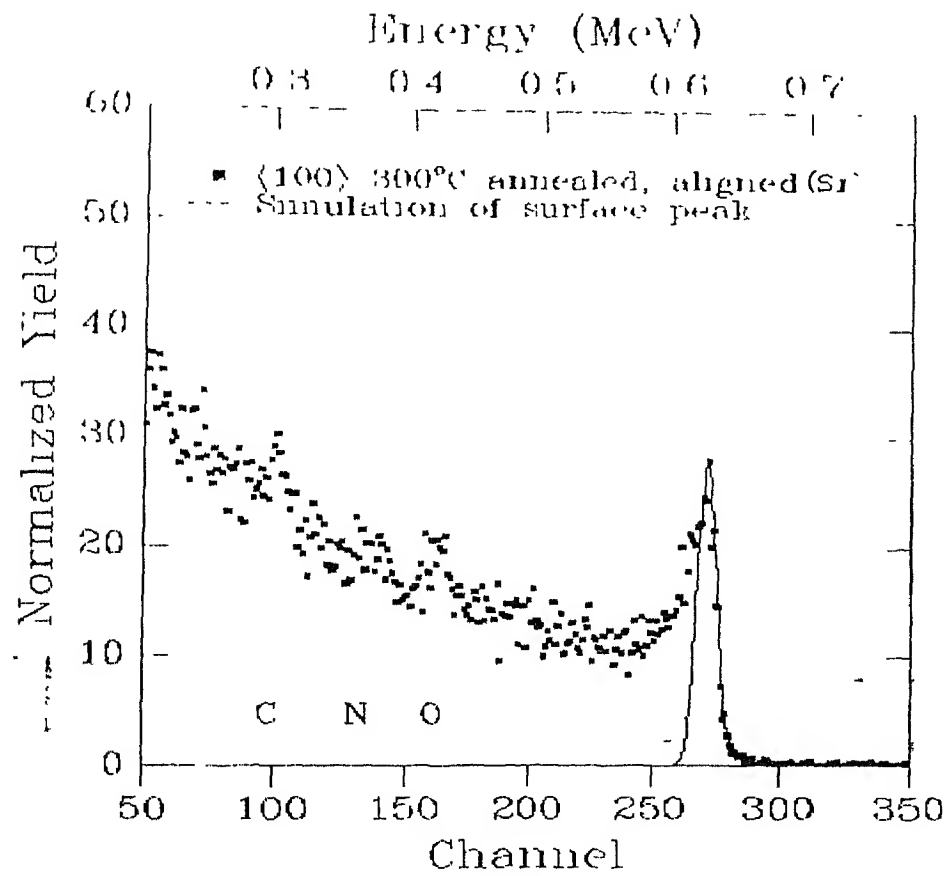


Fig. 4.10a. Simulated surface peak for aligned RBS spectrum of 300°C annealed Si.

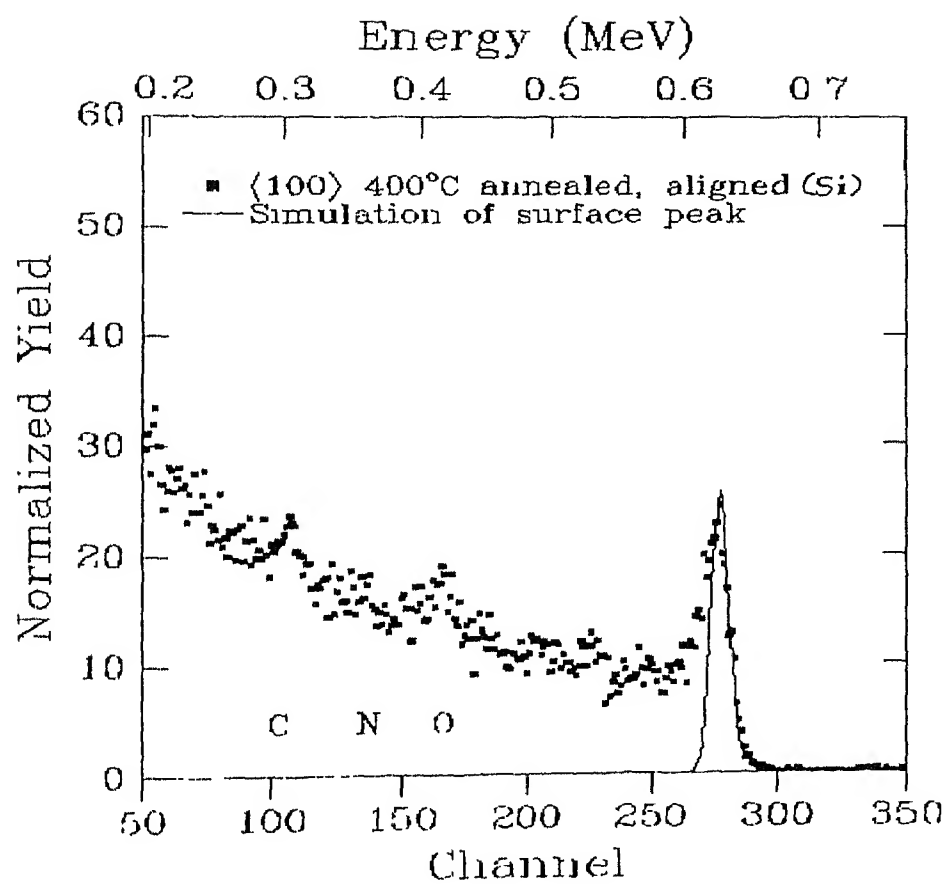


Fig. 4.10b. Simulated surface peak for aligned RBS spectrum of 400°C annealed Si.

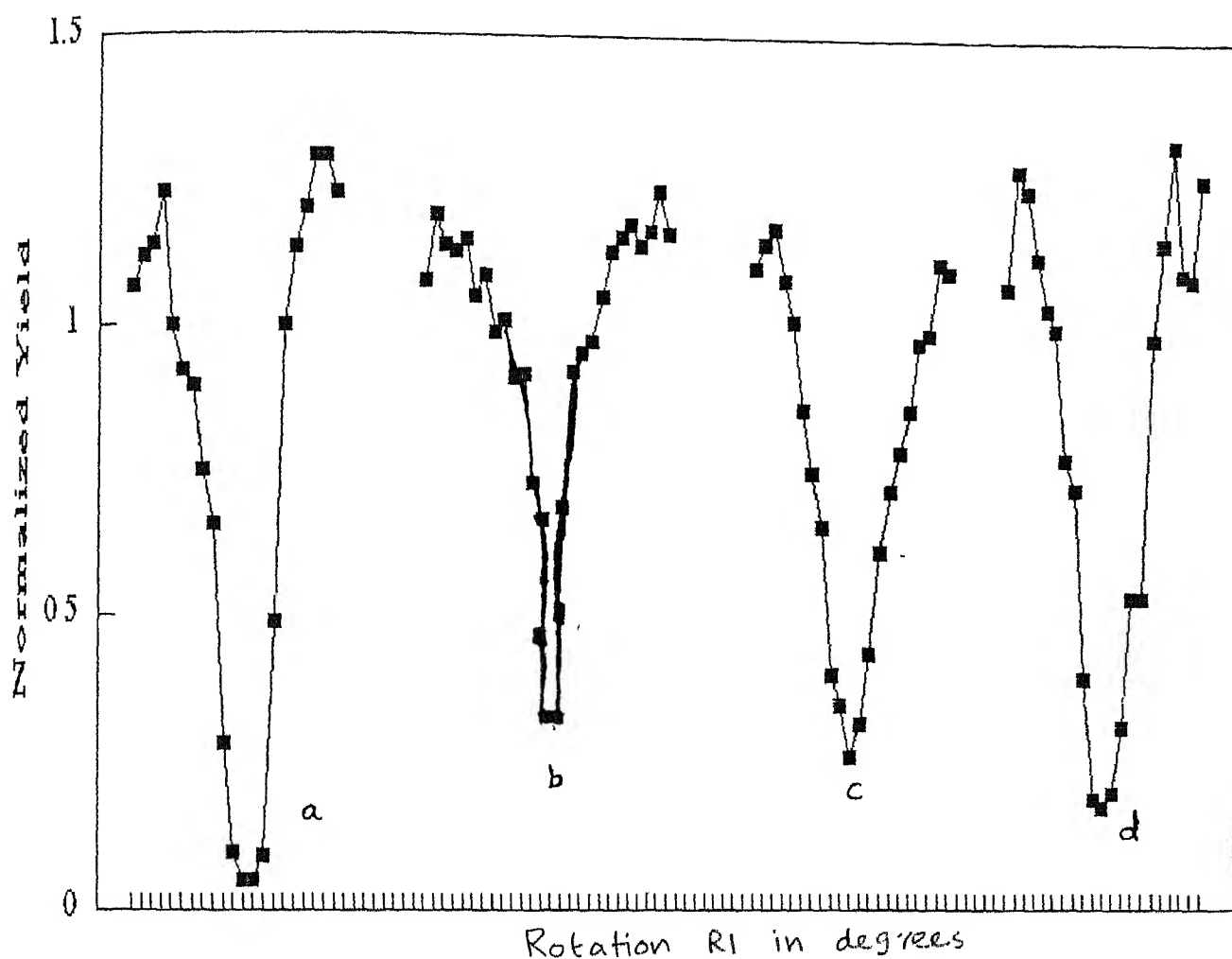


Fig. 4.11. Angular yield profiles for the Si (100) samples :

a) As-received,
c) 300°C annealed

b) 2 KeV nitrogen implanted,
d) 400°C annealed.

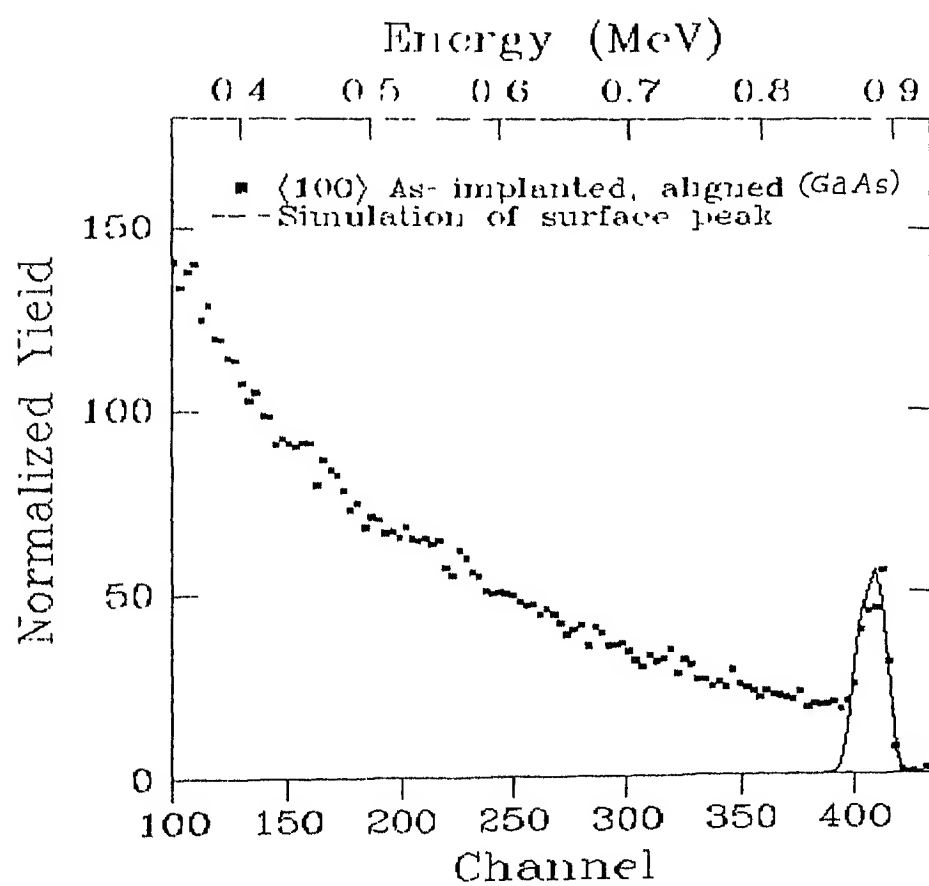


Fig. 4.13. Simulated surface peak for aligned RBS spectrum of 2 KeV nitrogen irradiated GaAs.

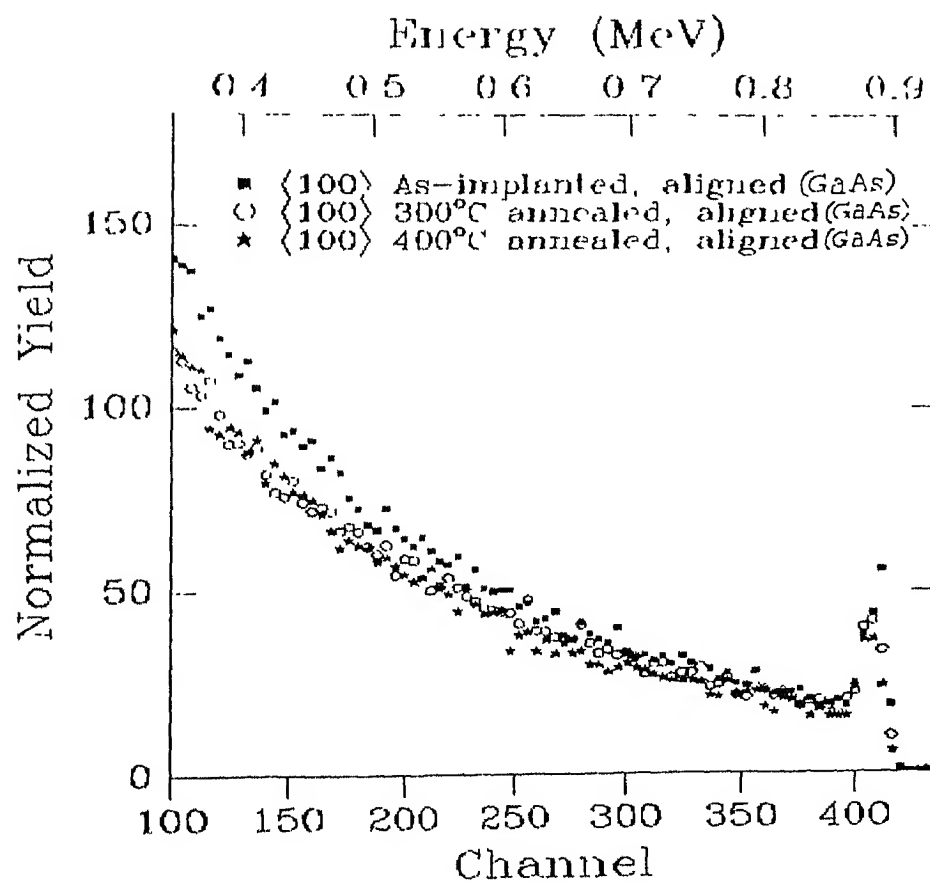


Fig 4.14. Aligned RBS spectra for the 300°C and 400°C annealed

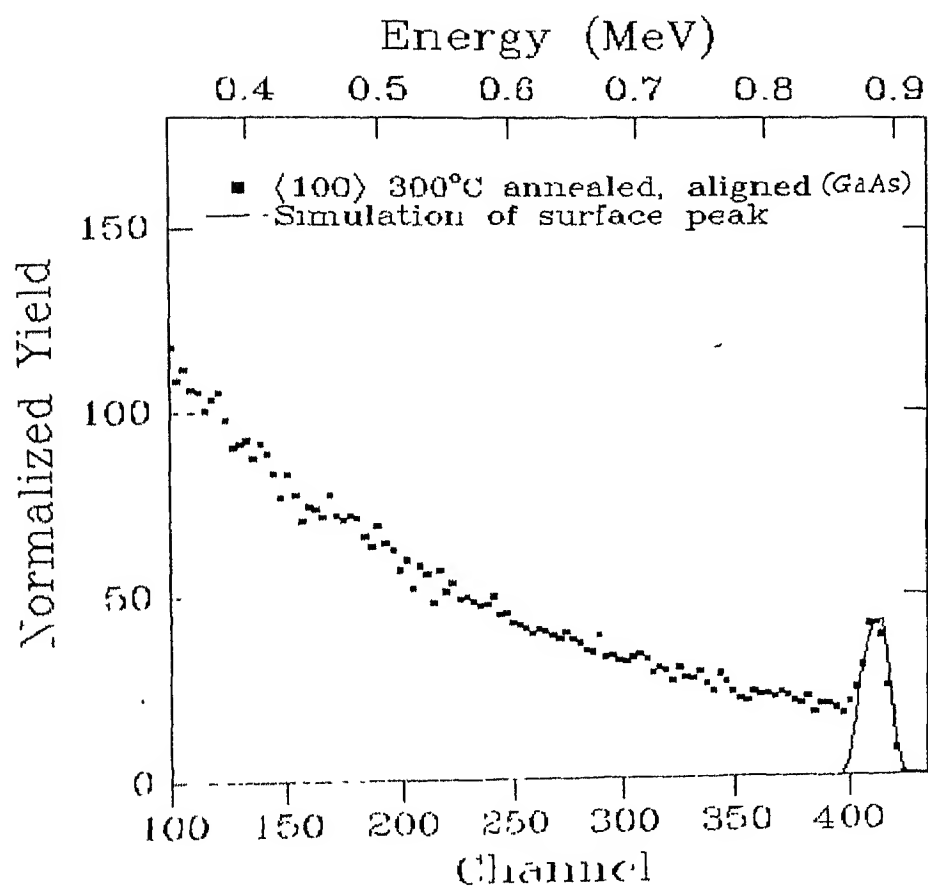


Fig. 4.15a. Simulated surface peak for aligned RBS spectrum of 300°C annealed GaAs.

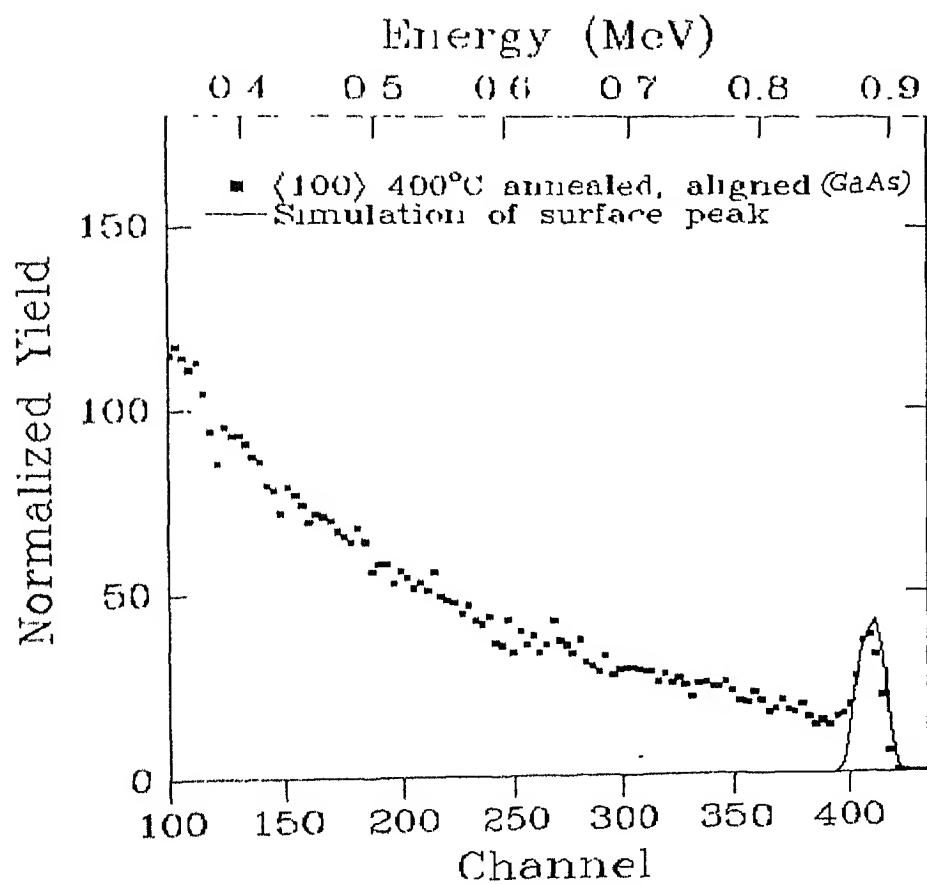


Fig. 4.15b. Simulated surface peak for aligned RBS spectrum of 400°C annealed GaAs.

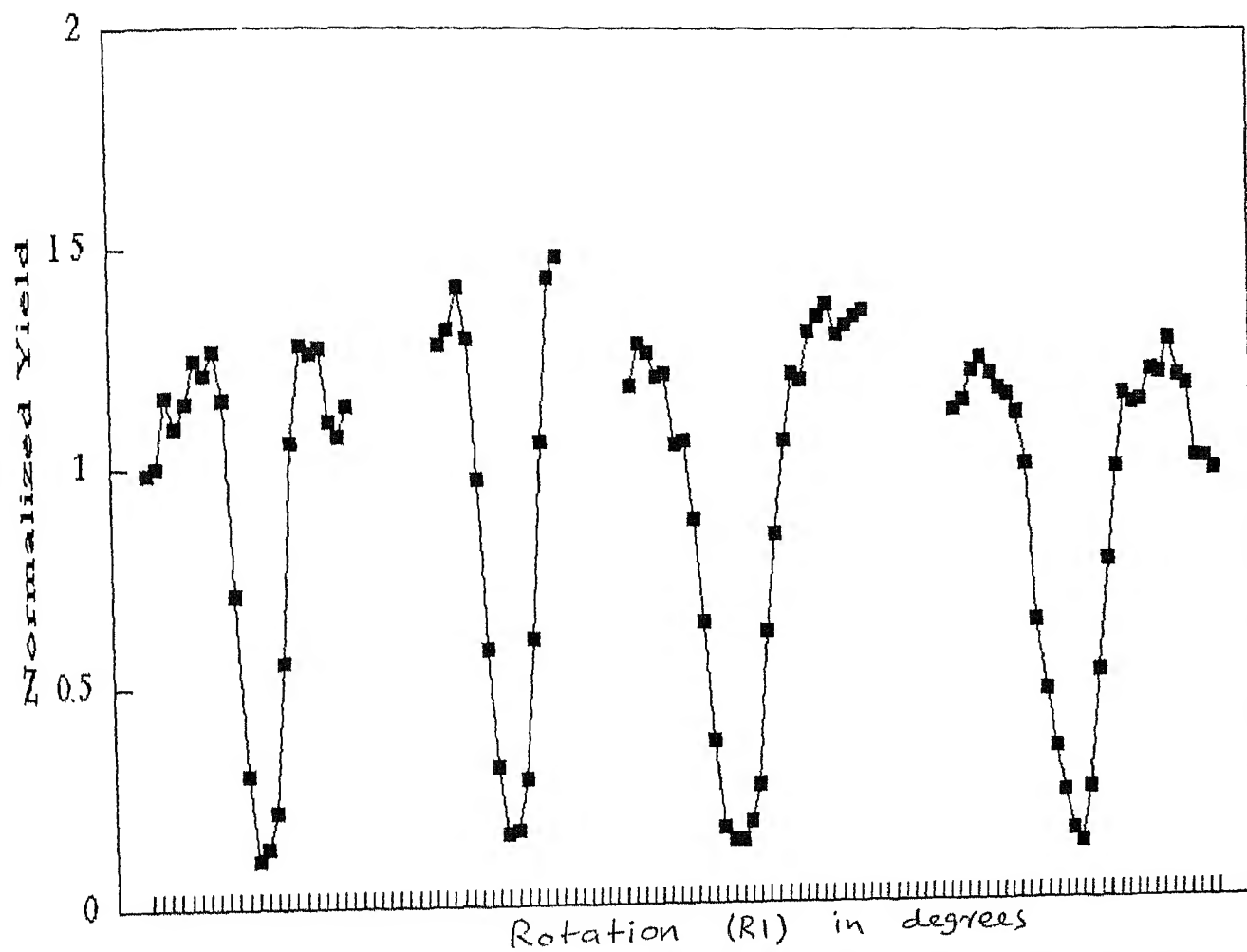


Fig. 4.16. Angular yield profiles for the GaAs (100) samples :

- | | |
|-------------------|------------------------------|
| a) As-received, | b) 2 KeV nitrogen implanted, |
| c) 300°C annealed | d) 400°C annealed. |

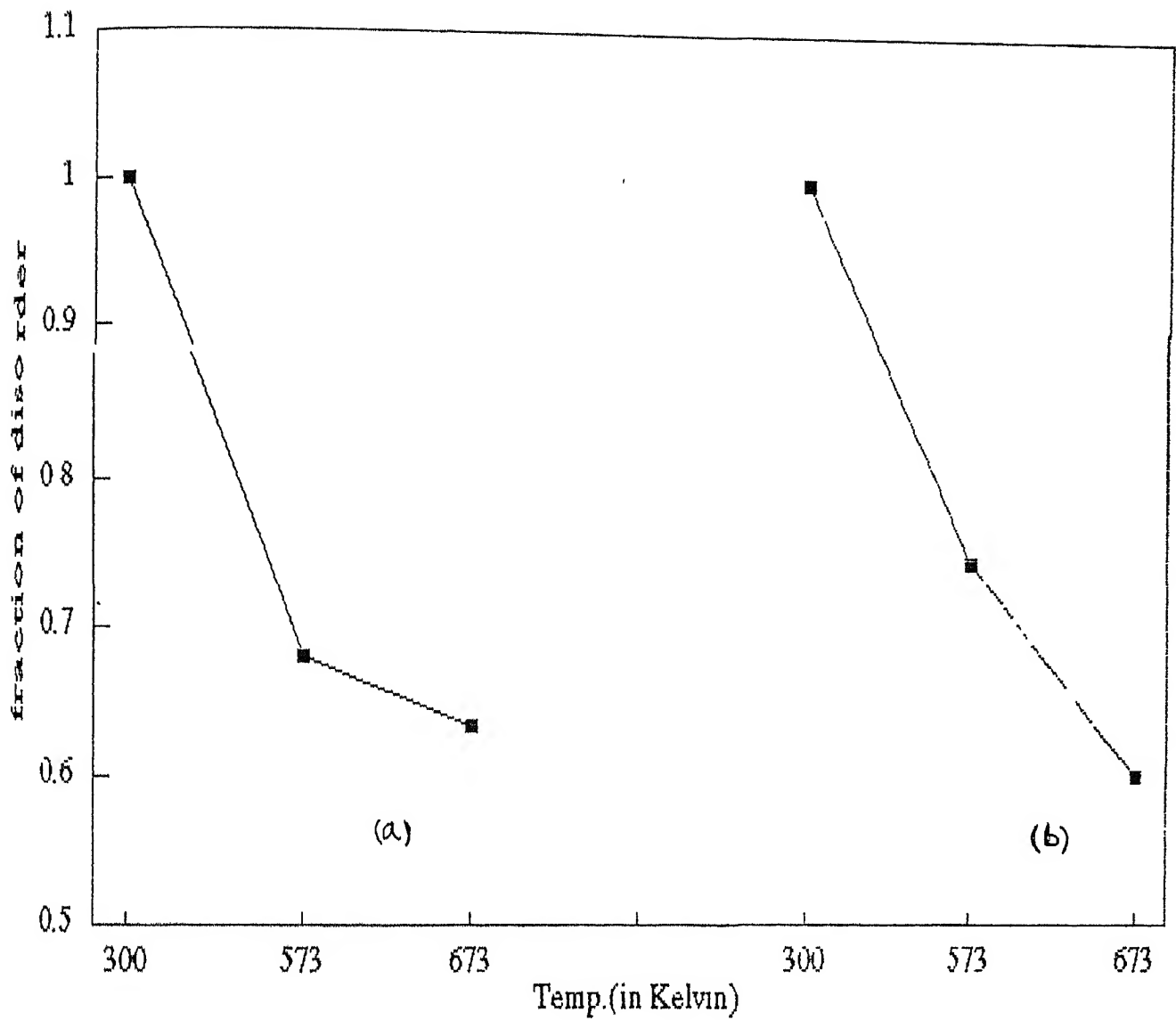


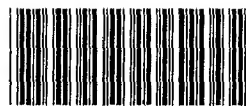
Fig. 4.17. Fraction of disorder remaining as a function of annealing temperatures in

a) GaAs (100)

b) Si (100).

A121242

MSP-1996-M-PAI-DEV



A121242